AD-A189 264 FLOW/ACOUSTIC INTERACTION IN DUCT INFLOW(U) ADMIRALTY RESEARCH ESTABLISHMENT TEDDINGTON (ENGLAND) M C QUINN SEP 87 ARE-TM-(UHA)-87511 DRIC-BR-103850 1/1

UNCLASSIFIED F/G 20/1 NL

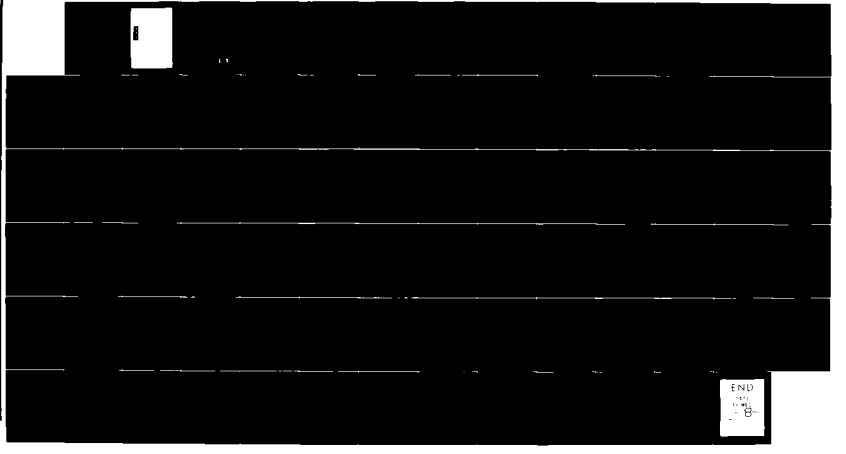

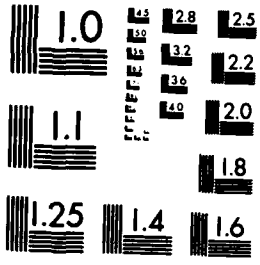

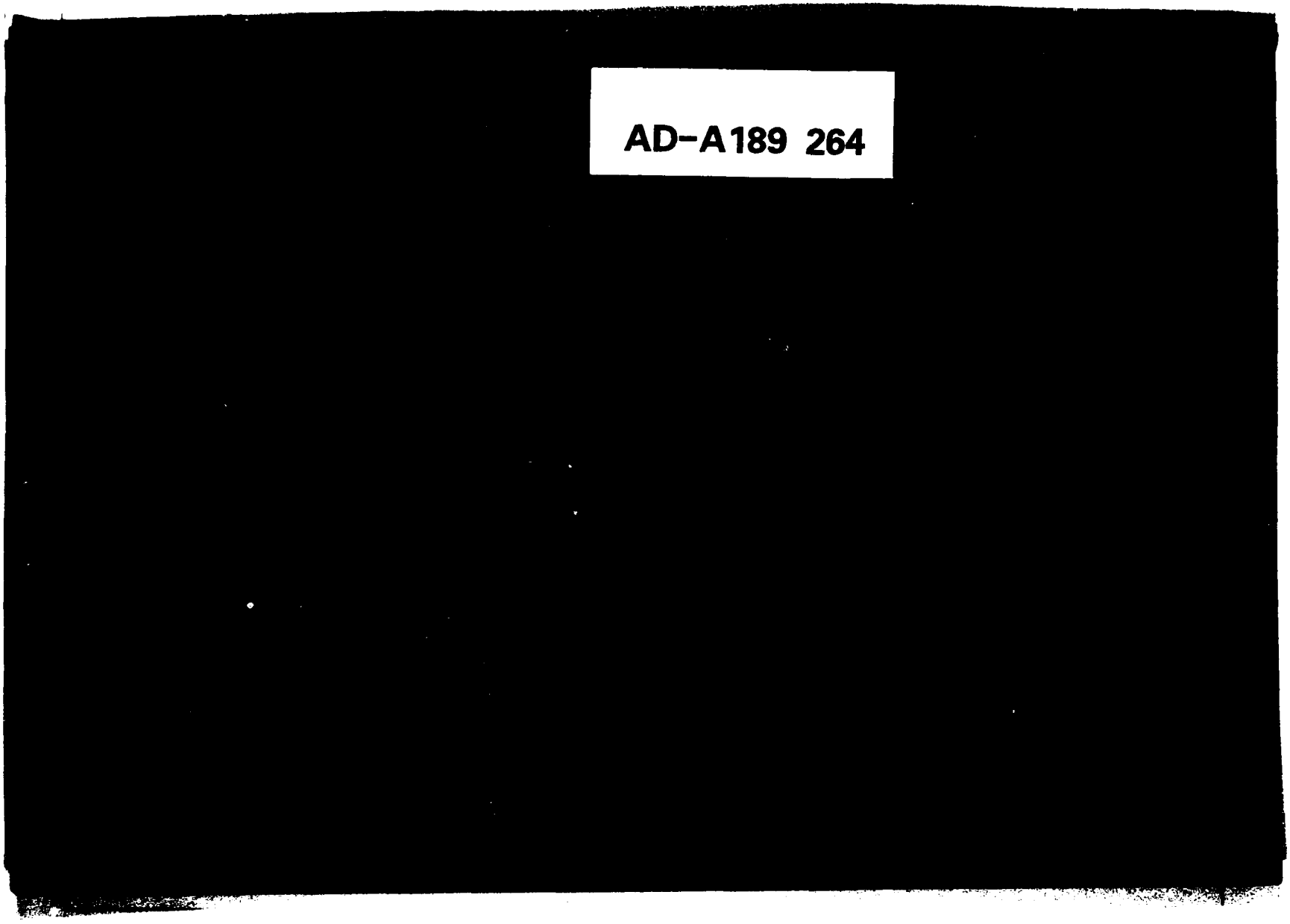

FLOW/ACOUSTIC INTERACTION IN DUCT INFLOW

by

M C Quinn

Abstract

Sound generation in the convection of turbulence into a flow intake duct is discussed by examination of an idealised problem. Ideal fluid is in motion with uniform low, subsonic velocity above and parallel to a plane, rigid wall. A thin, rigid, semi-infinite plate is parallel to the wall and the fluid flows past its leading edge. The radiated sound is calculated for a turbulent eddy modelled by a weak line vortex which is allowed to convect passively past the leading edge of the plate. Account is taken of the contribution to the radiated sound from the disturbance produced by the convecting vortex in the boundary layers on each side of the plate by means of Howe's (1981) theory of displacement thickness fluctuations, the strength of the disturbance being fixed by a leading edge Kutta condition. It is concluded that the predicted level of the radiated sound is substantially reduced due to the boundary layer disturbances relative to when they are neglected. The case of the convection of a frozen two-dimensional gust is also considered. Examination of the analogous problem of plane wave radiation from the duct shows that the presence of displacement waves enhanced both the far-field intensity in the ambient fluid and the reflected field within the duct.

Admiralty Research Establishment
Teddington
Queens Road
Teddington, Middx TW11 0LN

September 1987

79 pages
19 figs

C O N T E N T S

§1 Introduction.

Sound produced when a turbulent eddy is ingested by a duct inflow such as the intake duct of an engine or the entry of an exhaust nozzle, is of interest in many industrial systems. Of concern in similar circumstances are the sound fields which are radiated and reflected at the entry of a flow intake duct due to acoustic sources within the duct, such as a fan or propeller say. The flows of interest are often of low Mach number and the characteristic acoustic wavelength is large relative to the duct width.

The direct sound radiation from a compact turbulent eddy convected past a rigid body can be thought of as the sound which is produced in the absence of any interaction between the eddy and the flow in which it is convected. It is governed by the strain-field produced by the presence of the body, the details depending on the rate of working of the eddy turbulent stresses in that field (Howe 1975). For instance in the two-dimensional problem examined by Howe (1975) in which a line vortex moves around the edge of a thin semi-infinite rigid plate, no sound is produced if the vortex follows a potential flow streamline around the edge; sound is only produced when the vortex cuts across such streamlines.

In the presence of flow there are additional sound sources which are closely related to the incident vortical (or acoustic) disturbance. These arise because of flow/disturbance coupling at any edges of the object where vorticity can be generated and ejected into the flow, a process which is essentially viscous controlled. The mechanism provides a means of transferring energy that is well illustrated in

the impingement of a sound wave on the leading/trailing edge of a thin semi-infinite rigid plate in a low subsonic, grazing mean flow and respectively results in a net production/absorption of acoustic energy, Howe (1981).

In this paper we discuss sound production by the interaction of a vortical/acoustic disturbance with an otherwise uniform duct inflow. Though substantial amounts of acoustic energy can be produced when the incident flow is not self-preserving, as in the jet-edge tone configuration (Crighton 1984), in the cases examined here the disturbances are assumed to be sufficiently weak that both the disturbance and acoustic particle velocity are small relative to that of the mean flow.

The production of sound in the passive convection of a line vortex by a low Mach number mean flow, of speed U, past the mouth of a rigid, two-dimensional, semi-infinite duct is examined in §2. Longitudinal standing waves are avoided in this first analysis by considering a duct of infinite length. A more realistic model will also require a three-dimensional treatment to obtain predictions of the sound produced in the ingestion of a general turbulent field by a duct inflow. The duct is formed by an infinite plane rigid wall and a thin semi-infinite rigid plate, parallel to the wall and a distance H above it in the fluid. H is assumed small relative to any relevant acoustic wavelength. The mean flow Mach number $M = U/c$ (c is the sound speed) is small and, for convenience in the analysis, terms of order M^2 are neglected relative to unity. Thus c and the mean fluid density ρ can be taken as constant. The theory presented is linear with respect to the acoustic particle velocity.

The flow model is introduced in §2.1 and the analytical problem is formulated in §2.2. In §2.3 Howe's (1981) theory of displacement thickness fluctuations is applied to determine the effect on the radiated sound field of disturbances propagating in the plate boundary layers. Physically such disturbances arise from vorticity production at the plate leading edge by the action of viscosity in response to the unsteady velocity field of the passing vortex. The wall boundary layer is presumably well-established and stable, unlike the thin developing plate boundary layers which are linearly unstable. In the real flow, acoustic and thermal boundary layers, analogous to a Stoke's layer, will also be present on the plate and wall (due to the need to satisfy the no-slip condition at their respective surfaces) and will be extremely thin relative to an acoustic wavelength. Any interactions between vortex or sound shear waves, say, and boundary layer Reynold's stresses will be insignificant over the length and time scales which characterize the interaction of the vortex with the duct mouth and are neglected here. Similarly aerodynamic sound generation (Lighthill 1952) by mean or perturbed Reynold's stresses is not included. Thus it is not necessary to account for the boundary layer on the wall and the predominant effect of the plate boundary layer is accounted for by Howe's (1981) displacement wave theory.

In Howe's theory, fluctuations in the displacement thickness of the boundary layers model the effect of the disturbances in the exterior potential flow. Here, as in Howe (1981), the boundary layers are modelled as uniform wall flows of speed $V \ll U$ and the fluctuations are modelled as neutrally stable waves of constant form and of long wavelength relative to the characteristic boundary layer thickness. The displacement waves carry perturbation energy downstream into flow regions where they are dissipated by heat, viscosity or more

realistically perhaps, breakdown into small-scale turbulence. Thus the effective interaction region must be close to the leading edge of the plate. This physical assumption is incorporated into the analysis by allowing the wave-number of the displacement waves a small imaginary part where necessary to ensure the convergence of certain integrals. The strength of the displacement waves, proportional to that of the vortex, is fixed by the Kutta condition that the fluid velocity should remain finite at the plate leading edge. Viscous effects enter the analysis only in this indirect fashion.

Though the leading edge Kutta condition in unsteady flows has been examined by Goldstein (1981,1983) the issue of its validity has not been resolved. However Howe's (1981) application of the displacement wave theory incorporating the leading edge Kutta condition to the jet-drive mechanism of the flue organ pipe gives encouraging agreement with experiment. The edges of a real duct mouth will have finite thickness relative to the displacement wave length scale and may be rounded rather than sharp. Nevertheless the mechanism controlling the flow/acoustic interaction at the mouth will be essentially the same as that involving a thin plate. Goldstein (1984) shows that when a laminar flow separates from a smooth body surface and is subject to an external unsteady 'forcing' (e.g.,from a harmonic source), instability waves which propagate downstream are generated and are coupled to the source at the separation point by viscous effects. In particular for a harmonic source the Kutta condition is satisfied at the separation point provided that $1 \ll S \ll Re^{1/4}$, where S, Re are respectively the Strouhal and Reynold's numbers based on the streamwise body length scale and the upstream flow velocity. A comprehensive review of the Kutta condition in unsteady flows is provided by Crighton (1985).

The solution for a fourier time transform of the sound field is obtained in §2.4 by use of a low frequency Green's function and is found to have two components; the direct radiation from the vortex and the contribution from the displacement waves on the plate boundary layers. On application of the Kutta condition we find that the total field is simply the direct radiation multiplied by a factor equal to $(1-V/U_c) \simeq .4$, for a characteristic value of V/U_c where U_c ($\simeq U$) is the convection speed of the vortex. Thus the presence of displacement waves substantially reduces the radiated field. Comparison of the direct radiation is made with the solution obtained by Cannell and Ffowcs-Williams (1973) in the absence of mean flow for a line vortex exhausting out of the duct. Explicit forms of the far-field due to the line vortex, both in the duct and outside it, are obtained in §2.5 and are valid when the duct is wide relative to the displacement wave length scale, characterised by the minimum distance of the vortex from the plate. This shows that it makes little difference whether the vortex moves above the plate or beneath it into the duct.

The results of §2.5 are used in §2.6 where the radiated field produced in the convection into the duct of an incompressible, frozen two-dimensional gust is discussed. The flux of acoustic energy, both to the far-field in the duct and outside it, is calculated in §2.6. For the line vortex case these fluxes are compared; the former is proportional to M, the latter to M^2.

In §3 a low frequency plane sound wave propagating out of the duct replaces the line vortex as the 'incident' sound source. The displacement wave theory outlined above is employed. In this case the presence of displacement waves results in an increase in both the far-field intensity outside the duct and the amplitude of the reflected

field within the duct. There is experimental evidence (Davies 1987) of such an increase in the reflection coefficient in plane wave reflection at a flow intake. The calculation of §3.2 reveals that the net acoustic energy flux away from the plate leading edge is positive; acoustic energy is generated by the displacement thickness waves. This is in accord with the results of Howe (1981) for the interaction of a plane wave with a plate leading edge and of Quinn & Howe (1986). Appendices A1-A4 contain various analytical results.

§2 Sound generation by convection of turbulence

§2.1 The flow model

The problem to be considered is illustrated schematically in figure 1. A uniform mean flow of low, subsonic velocity U proceeds along a rigid wall (at $x_2 = 0$ in the (x_1, x_2) co-ordinate system of the figure) and encounters a two-dimensional duct formed by a thin, rigid semi-infinite plate at $x_2 = H$ above the wall. A turbulent eddy modelled by a line vortex of strength $\gamma/2\pi$ convects at speed U_c along a path $x_2 = h$. Since the flow Mach number satisfies $M = U/c \ll 1$, the speed of sound in the fluid, c, may be assumed constant and in the subsequent analysis terms of order M^2 are neglected relative to unity.

The aim of the analysis is to provide estimates of the sound produced by the interaction of the vortex with the duct mouth. Besides the 'direct radiation' from the vortex there are acoustic sources closely related to the vortex which arise when, in response to the velocity field of the passing vortex, additional vorticity is ejected into the plate boundary layers at the plate leading edge. The assumed region of this interaction is indicated schematically by the wavy lines in figure 1. The flow region of importance to the acoustic far-field is assumed to be the vicinity of the duct mouth, $|x| < H$, and should be confirmed by the results of the analysis.

The turbulent boundary layers on the wall and plate will be extremely thin relative to the acoustic wavelengths concerned and

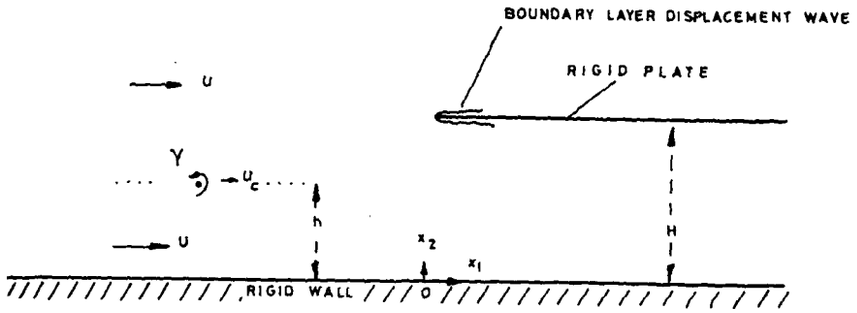

Figure 1. Schematic illustration of convection of a line vortex by a uniform mean flow into a semi-infinite duct.

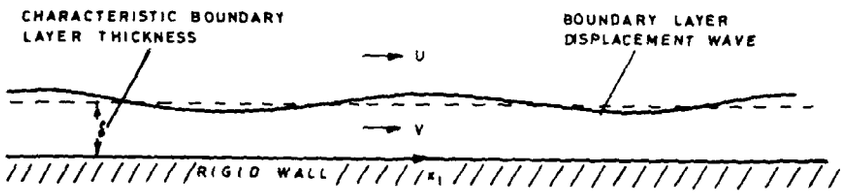

Figure 2. Sketch of the idealized boundary layer model with a displacement wave.

their interactions with the acoustic fields produced are assumed to be incoherent in respect to the acoustic time and length scales of interest. The line vortex is assumed to be sufficiently weak, compact and incoherent with regard to the turbulent boundary layers that additional sound fields arising from perturbed Reynolds stresses can be neglected. Thus the wall boundary layer is excluded and the plate boundary layers enter the model only in relation to the leading edge interaction outlined above.

The fluid mechanics governing the vortex is of interest only in the effective interaction region, $|x| < H$ where the vortex (or gust of §2.5) is assumed to convect passively at a speed U_c. Variations in U_c and curvture in the vortex path during the passage of the vortex past the duct mouth due to an image system in the plate will be small provided that $\gamma/|H-h| << U_c$ and are neglected. A physically realistic convected disturbance might have a convection velocity of .5U to .8U. The simplistic modelling of the vortex means that the energetics of the interaction, being of second order in the acoustic fluctuations produced, is not included explicitly in the flow model. Radiated acoustic energy produced in the interaction is balanced by a decrease in mean flow energy or energy of the convected disturbance which in the real flow might be expected to be apparent in higher turbulence levels in the plate boundary layers downstream of the edge.

In addition to $M << 1$ further physically acceptable but limiting assumptions enter the analysis. Since typically turbulence levels will not exceed 10% of the mean flow velocity we take $u_h << U$, u_h being the characteristic hydrodynamic disturbance velocity. The acoustic particle velocity, $|\nabla\phi|$ (ϕ is a perturbation potential) will also be small relative to U and $U_c = O(U)$. These inequalities may be

expressed as $|\nabla\phi|$, $u_n \ll U \ll c$. The neglect of terms of order M^2 relative to unity is for mathematical convenience. The assumption of an acoustically compact interaction region should be satisfied provided that the duct height is small relative to any relevant acoustic wavelength, i.e. $H \ll c/\omega$ for a characteristic radian frequency ω. Effects due to thermal diffusion processes can be assumed to be insignificant in view of the relatively short time envisaged for the passage of the disturbance through the region $|\underline{x}| < H$.

§2.2 The analytical problem

Given this modelling we consider the analytical problem illustrated schematically in figure 1; ideal fluid is in motion in the positive x_1 direction of the (x_1, x_2) co-ordinate system with uniform low, subsonic velocity U above a rigid wall at $x_2 = 0$. A thin rigid semi-infinite plate is at $x_2 = H$, $x_1 > 0$ and is parallel to the wall. A line vortex of strength $\gamma/2\pi$ convects at a constant speed U_c at a constant distance h above the wall.

When visco-thermal effects are neglected the stagnation enthalpy $B(\underline{x}, t)$, defined by

$$B = w + v^2/2 \qquad (2.1)$$

where w is the specific enthalpy and $\underline{v}$ is the fluid velocity, will satisfy the inhomogeneous convected wave equation (Howe, 1975);

$$\left[\frac{\partial^2}{\partial x_1^2} + \frac{\partial^2}{\partial x_2^2} - \left(\frac{1}{c}\frac{\partial}{\partial t} + M\frac{\partial}{\partial x_1}\right)^2\right] B(\underline{x},t) = -\mathrm{div}(\underline{\omega} \times \underline{v}). \qquad (2.2)$$

B is employed here as the fundamental acoustic variable. In equation (2.2) $\underline{\omega} = \mathrm{curl}\underline{v}$ is the vorticity, c is the speed of sound and may be assumed to be constant since the Mach number $M = U/c$ of the flow satisfies $M^2 \ll 1$. In irrotational flow regions we may take

$$B = -\partial\phi/\partial t \qquad (2.3)$$

where ϕ is a perturbation potential of the flow.

The source term in (2.2) will be non-zero only in vortical flow regions, i.e. at the vortex core given by $x_1 = U_c(t-t_o)$, $x_2 = h$ (where t_o is a constant) and possibly at the surfaces of the plate $x_2 = H \pm \varepsilon$, where additional vorticity may be introduced into the flow at the leading edge by the passing line vortex. The vorticity of the convecting line vortex, ω_l, say is

$$\omega_l = \gamma\, \delta(x_1 + U_c t_o - U_c t)\, \delta(x_2 - h)\, \underline{e} \qquad (2.4a)$$

where $\underline{e}$ is a unit vector out of the plane of the paper in figure 1 and δ is the Dirac delta function. ω_l can be expressed as a superposition of vorticity waves:

$$\omega_l(\underline{x},t) = \int_{-\infty}^{\infty} \hat{\omega}_l(\underline{x},t,\omega)\,d\omega \,,$$

where $\qquad (2.4b)$

$$\hat{\omega}_l = (\gamma/2\pi U_c)\delta(x_2-h)\exp(i\omega[t_o - t + x_1/U_c])\underline{e} \,.$$

Henceforth hatted quantities will denote variables in the frequency domain and the time dependence $\exp(-i\omega t)$ will not be denoted explicitly. The solution for the stagnation enthalpy, B can be obtained by superposition of the solution, $\hat{B}$ say, associated with the vortical field $\hat{\underline{\omega}}_1$ of (2.4b). We note that

$$\hat{\underline{\omega}}_1 \times \underline{v} = (\gamma/2\pi)\delta(x_2-h)\exp(i\omega[t_o+x_1/U_c])\underline{n} \ , \qquad (2.5)$$

where $\underline{n}$ is a unit vector in the positive x_2 direction of figure 1.

§2.3 Boundary Conditions

The far-field radiated sound will be calculated from equation (2.2) with the incident vorticity field $\hat{\underline{\omega}}_1$ of (2.4b) and appropriate boundary conditions at the plate and wall. On the rigid wall, $x_2 = 0$, the zero normal velocity condition requires that $\partial\hat{B}/\partial x_2 = 0$, since from (2.3) and (2.4b), $\hat{B} = i\omega\hat{\phi}$. The same condition applied on the plate, $x_1 > 0$, $x_2 = H$ would lead to singularities in the velocity and pressure at the plate leading edge, $\underline{x} = (0,H)$. The singularities result from the idealization that viscous effects are negligible whereas in practice viscosity acts to inhibit such singular behaviour. The singularities are avoided here by use of Howe's (1981) theory of displacement thickness waves. In that theory the effect on the exterior potential flow of large scale boundary layer disturbances (produced by vorticity generated at the leading edge) is modelled by fluctuations in the displacement thickness of the boundary layers emanating from the edge. Greater detail of the theory is given by Howe (1981) where an idealized model of the boundary layer, sketched in figure 2 and adopted here, is employed. In the model a boundary

layer wave of the form $A\exp(i\chi x_1)$, $\chi = \chi(\omega)$, propagates above a uniform wall flow of speed V with $V < U$, U being the speed of the exterior uniform flow. Howe shows that though a wide range of values of $\chi(\omega)$ are possible for each ω, as $\chi\delta \to 0$ (δ is the characteristic boundary layer thickness) the various modes coalesce and $\chi \to \omega / V$. We take

$$\chi = \omega / V \tag{2.7}$$

and suppose that $V = 0.6U$, a value suggested by the work of Bull (1967) and Blake (1970). Thus the boundary condition at control surfaces defined by $x_2 = H\pm\delta$, $x_1 > 0$, just outside the thin boundary layers on the plate is

$$\partial\hat{B}/\partial x_2 = i\omega\nu(\omega)\exp(i\chi x_1), \quad x_1 > 0, \quad x_2 = H\pm 0, \tag{2.8}$$

where $\nu(\omega)$, a measure of the strength of the disturbances in the boundary layers, is to be fixed by the Kutta condition that the fluid velocity is finite at the leading edge. In (2.8) it has been assumed that the condition can be applied on the surface of the plate.

§ 2.4 The solution for a vortex wave

Introduce the degenerate Prandtl-Glauert transformation (in which M^2 is neglected relative to unity)

$$\vec{B}(\underline{x}) = \hat{B}(\underline{x})\exp(i\omega U x_1/c^2), \tag{2.9}$$

The governing wave equation (2.2) becomes

$$\left[\frac{\partial^2}{\partial x_1^2} + \frac{\partial^2}{\partial x_2^2} + \frac{\omega^2}{c^2}\right] \tilde{B}(\underline{x}) = -\mathrm{div}(\hat{\underline{\omega}} \times \underline{y})\exp(i\omega U x_1/c^2) \ , \qquad (2.10)$$

where again M^2 has been neglected relative to unity. We define $G(\underline{x};\underline{y})$ as the solution of

$$\left[\frac{\partial^2}{\partial y_1^2} + \frac{\partial^2}{\partial y_2^2} + \frac{\omega^2}{c^2}\right] G(\underline{x};\underline{y}) = -\delta(\underline{x}-\underline{y}), \qquad (2.11)$$

satisfying

$$\partial G/\partial y_2 = 0, \quad y_2 = 0, \quad |y_1| < \infty \ ,$$

$$\partial G/\partial y_2 = 0, \quad y_2 = H, \quad y_1 > 0 \ , \qquad (2.12)$$

and the radiation condition that $G(\underline{x};\underline{y})$ should have outgoing wave behaviour in $\underline{y}$ space for $\omega|\underline{y}|/c >> 1$, and that as $y_1 \to \infty$ with $|y_2| < H$, $G(\underline{x};\underline{y}) \to \text{constant}.\exp(i\omega y_1/c)$. $G(\underline{x};\underline{y})$ is calculated in Appendix A2.

From equations (2.10), (2.11) we find

$$\tilde{B}(\underline{x}) = \int_V (G(\underline{x};\underline{y})\nabla^2\tilde{B}(\underline{y}) - \tilde{B}(\underline{y})\nabla^2 G(\underline{x};\underline{y}) + G(\underline{x};\underline{y})\mathrm{div}(\omega\underline{x}\underline{y})\exp(i\omega U y_1/c^2))\ dV. \qquad (2.13)$$

The integration in (2.13) is over the region of fluid V' which is enclosed by a control surface S. S consists of the rigid wall $y_2 = 0$, a surface $y_1 = \text{constant} = \infty$ for $|y_2| < H$, control surfaces at $y_2 = H+\delta$

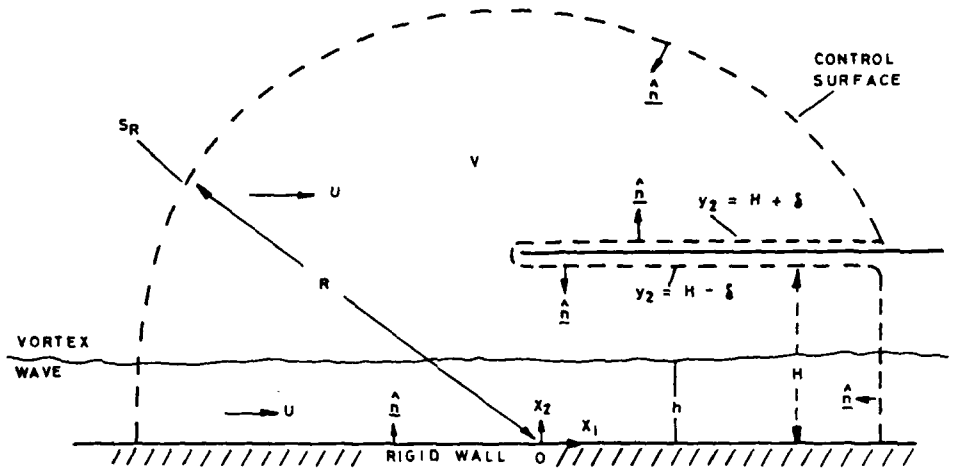

Figure 3. Sketch of the control surfaces of equation (2.14) and the vortex wave.

for $y_1 > 0$ (around the plate) and a circular arc centred on (0,H) to give a closed circuit. Application of Green's theorem to the fluid within S gives from (2.13)

$$\tilde{\mathbf{B}}(\mathbf{x}) = -\int_S \mathbf{n}.\{G(\mathbf{x};\mathbf{y})\nabla\tilde{\mathbf{B}}(\mathbf{y}) - \tilde{\mathbf{B}}(\mathbf{y})\nabla G(\mathbf{x};\mathbf{y}) + G(\mathbf{x};\mathbf{y})(\omega\mathbf{x}\mathbf{y})\exp(i\omega U y_1/c^2)\}dS$$

$$- \int_V (\omega \times \mathbf{y}).\nabla\{G(\mathbf{x};\mathbf{y})\exp(i\omega y_1/c^2)\}\, dV\,, \qquad (2.14)$$

where (see figure 3) $\mathbf{n}$ is the unit normal to S in the direction of the interior of S. Noting that vortical fluid enclosed by S is that of the vorticity wave, we find on using the radiation conditions on $G(\mathbf{x};\mathbf{y})$ and the conditions (2.12) that

$$\tilde{\mathbf{B}}(\mathbf{x}) = -\int_0^\infty \left\{G(\mathbf{x};\mathbf{y})\underline{\underline{1}}^{+}\frac{\partial\tilde{\mathbf{B}}(\mathbf{y})}{\partial y_2}\right\}\Big|_{y_2=H} dy_1 - \frac{\gamma\exp(i\omega t_0)}{2\pi}\int_{-\infty}^{\infty}\frac{\partial G(\mathbf{x};\mathbf{y})}{\partial y_2}\exp(i\omega y_1(1+MU_c/c)/U_c)\Big|_{y_2=h} dy_1\,.$$

(2.15)

where continuity in $\partial B/\partial y_2$ across the plate (c.f. (2.8)) has been used. In this equation the first integrand is evaluated at $y_2 = H$, the second at $y_2 = h$. We have used equation (2.5) for the term $(\omega \times v)$ and the notation

$$\{f\underline{\underline{1}}^{+} = f(y_1,H+0) - f(y_1,H-0). \qquad (2.16)$$

The plate boundary condition (2.8) is substituted in (2.15) and the Prandtl-Glauert transformation (2.9) reversed to give the actual enthalpy as

$$\hat{B}(\underline{x}) = \hat{B}_{\omega}(\underline{x}) + \hat{B}_{w}(\underline{x}), \tag{2.17}$$

where

$$\hat{B}_{\omega}(\underline{x}) = \frac{-\gamma \exp(i\omega(t_o - Ux_1/c^2))}{2\pi} \int_{-\infty}^{\infty} \exp((i\omega y_1)[1+MU_c/c]/U_c) \frac{\partial G(\underline{x};y_1,h)}{\partial y_2} dy_1 , \tag{2.18}$$

$$\hat{B}_{w}(\underline{x}) = -i\omega\gamma \exp(-i\omega Ux_1/c^2) \int_{o}^{\infty} \exp(i\chi y_1 + i\omega Uy_1/c^2) [G(\underline{x};\underline{y})]_{\underline{1}}^{\dagger} dy_1 . \tag{2.19}$$

$\hat{B}_{\omega}(\underline{x})$ is the direct contribution to the sound field from the vorticity wave of (2.4b) while $\hat{B}_{w}(\underline{x})$ is due to the disturbed boundary layers on the plate. The integrals of (2.18), (2.19) are approximated by use of equation (A2.9) of Appendix A2 which is valid for positions $\underline{x}$ in the far-field, $\underline{y}$ in the near-field and gives

$$[G(\underline{x};\underline{y})]_{\underline{1}}^{\dagger} = \alpha(\underline{x},\omega)[\underline{\Phi}(\underline{y})]_{\underline{1}}^{\dagger} ,$$

$$\partial G(\underline{x};\underline{y})/\partial y_2 = \alpha(\underline{x},\omega)\partial\phi(\underline{y})/\partial y_2 , \tag{2.20a,b}$$

for $\omega|\underline{x}|/c \gg O(1)$, $\omega|\underline{x}|/c \ll O(1)$. $\bar{\Phi}$ is a potential function of an inflow into the duct (uniform when $|y_2|<H$, $y_1 \to \infty$) and is discussed in Appendix A1. α is the function

$$\alpha(\underline{x},\omega) = \frac{-\omega}{2c}\frac{(H_0^{(1)}(\omega|\underline{x}|/c)+i(x_1/|\underline{x}|)H_1^{(1)}(\omega|\underline{x}|/c))}{(1+i\omega Hf(\omega)/\pi c)} , \qquad (2.21a)$$

with

$$f(\omega) = .5772-i\pi/2+\ln(\omega H/2\pi c). \qquad (2.21b)$$

(c.f (A2.8), (A2.12) of Appendix A2). $H_0^{(1)}$, $H_1^{(1)}$ are Hankel functions of the first kind. The term involving $H_0^{(1)}$ is a monopole scattered field and that involving $H_1^{(1)}$ is a dipole scattered field.

(i) To evaluate $\hat{B}_\omega(\underline{x})$: the direct radiation

Equations (2.20b) and (2.19) give (with results (A1.4), (A1.6) of Appendix A1)

$$\hat{B}_\omega(\underline{x}) = (\gamma/2\pi)\mathcal{K}\alpha(\underline{x},\omega)\exp(i\omega(t_0-Mx_1/c)) , \qquad (2.22a)$$

where (c.f definition (A4.9) of Appendix A4)

$$\mathcal{K} = \int_{-\infty}^{\infty}\exp(i\omega y_1/U_c)\ln(1/(1-Z_0^2))dy_1 , \qquad (2.22b)$$

and $Z_0(y_1)$ is the image of the point y_1+jh, $j=(-1)^m$, under the transformation (A1.2) of Appendix A1. $\hat{B}_\omega(\underline{x})$ corresponds to the radiated field calculated by Cannell and Ffowcs-Williams (1973), by

means of matched asymptotic expansions, for the case when a vortex exhausts from the duct in the absence of mean flow, its motion due to images in the duct walls. Equation (2.22a) agrees with their results when account is taken of the different vortex motions, save that the term $f(\omega)$ in $\alpha(\underset{\sim}{x},\omega)$ of (2.21) is absent in their calculation. The discrepancy appears to arise because of their erroneous exclusion of a pressure variation which is uniform over the whole duct mouth (c.f. equation (3.15) of Cannell and Ffowcs-Williams (1973)).

(ii) To evaluate $\hat{\underset{\sim}{B}}(\underset{\sim}{x})$: the displacement wave contibution

Neglecting M^2 relative to unity, we find from (2.19), (2.20a) that

$$\hat{\underset{\sim}{B}}(\underset{\sim}{x}) = -i\omega\nu(\omega)\exp(-i\omega Mx_1/c)\alpha(\underset{\sim}{x},\omega)\int_C \exp(i\chi y_1)[\underset{\sim}{\phi}]^+ \, dy_1$$

$$= i\omega\nu(\omega)\exp(-i\omega Mx_1/c)\alpha(\underset{\sim}{x},\omega)\int_{-\infty}^{\infty} \frac{\underset{\sim}{\phi}}{i\chi d\underset{\sim}{\phi}} \, d(\exp(i\chi y_1)) \, d\underset{\sim}{\phi}\Big|_{y_2=+} , \qquad (2.23)$$

where now the integration variable is the potential $\underset{\sim}{\phi}$. The displacement waves must decay as $y_1 \to \infty$ due to dissipation by heat and viscosity, or breakdown into turbulence, and this is modelled here by allowing ω a small positive imaginary part (for $\omega>0$) in the evaluation of the integral of (2.23) to give

$$\hat{\underset{\sim}{B}}(\underset{\sim}{x}) = -(\omega\nu(\omega)/\chi)\exp(-i\omega Mx_1/c)\alpha(\underset{\sim}{x},\omega)\int_{-\infty}^{\infty} \exp(i\chi y_1) d\underset{\sim}{\phi} .$$

Comparison with (A4.5) of Appendix A4 leads to the result

$$\hat{B}_{-}(\underline{x}) = -(\omega\psi(\omega)H/\chi\pi)\exp(-i\omega Mx_1/c)\alpha(\underline{x},\omega)\exp[L(-i\chi H/\pi)] \quad . \qquad (2.24)$$

where

$$L(x) = \ln[T(x)] - x\ln x + x \quad , \qquad (2.25)$$

and T is the gamma function (Gradshteyn and Ryzhik 1980, p933).

The calculation of Appendix A4 fixes $\psi(\omega)$ by application of the Kutta condition that the fluid velocity remain finite at the plate leading edge and gives (c.f. equation (A4.10))

$$\psi(\omega) = \pi(\gamma/2\pi)\exp[i\omega t_o - L(-i\chi H/\pi)]K/HU_c \quad . \qquad (2.26)$$

On substitution in (2.24) we find

$$\hat{B}_{-}(\underline{x}) = -(V/U_c)(\gamma/2\pi)K\alpha(\underline{x},\omega)\exp(i\omega[t_o - Mx_1/c) \quad , \qquad (2.27)$$

which is valid in the far-field, $\omega|\underline{x}|/c >> 1$. Comparison with (2.22) reveals that

$$\hat{B}(\underline{x}) = \hat{B}_{+}(\underline{x}) + \hat{B}_{-}(\underline{x}) = (1-V/U_c)\hat{B}_{+}(\underline{x}) \quad . \qquad (2.28)$$

The term containing V arises from the displacement waves so their presence has the effect of reducing the level of the radiated sound by a factor of $(1-V/U_c)$ which for a characteristic value of $V = 0.6U$ and $U_c = U$ is 4'10. The reduction is greater if $U_c < U$ and for $V = U_c$ no sound is radiated, as if the plate were absent. It is interesting to

compare this result with those of Howe (1976) for the case when a line vortex convects past the trailing edge of a thin semi-infinite rigid plate in a low subsonic grazing mean flow. Application of the trailing edge Kutta condition required vorticity to be shed from the edge and to convect at the mean flow velocity in a vortex sheet wake downstream from the edge. Howe found that no sound was radiated if the convection velocity of the vortex and shed vorticity were equal.

§2.5 The solution for a convected line vortex upstream disturbance

The stagnation enthalpy $B(\underline{x},t)$ for the line vortex of (2.4a) is obtained by integration of $B(\underline{x})$ over ω. We suppose that the duct is extremely wide on the hydrodynamic length scale U/ω, in which case the integral K of (2.26b) is approximated by equation (A4.14) of Appendix A4. We find from (2.22), (2.28) that

$$B(\underline{x},t) \simeq (1-V/U_c)(\gamma/4\pi)(HU_c)^{\infty}(1-i)\int_{-\infty}^{\infty} \frac{\alpha(\underline{x},\omega)\exp(-i\omega\bar{t})[\exp(-\omega HX/U_c)]\Big|_{X-}^{X+}}{|\omega|^{\infty}}\, d\omega + c.c \tag{2.29}$$

where

$$\bar{t} = t - t_o + Mx_1/c, \tag{2.30}$$

and

$$X_+ = |1-h/H|, \quad X_- = (1+h/H).$$

The difference in the integrand is to be taken between $X=X_+$, c.c denotes the complex conjugate of the preceding expression and we have

used $\alpha^*(\underline{x},\omega)=\alpha(\underline{x},-\omega)$, $K^*(\omega)=K(-\omega)$ (c.f. (2.21) and (2.22b)). An asterisk denotes the complex conjugate.

(i) Far-field outside the duct

On substitution for $\alpha(\underline{x},\omega)$ from (2.21) into (2.29) we obtain

$$B(\underline{x},t) = \frac{(1-V/U_c)\gamma M_c^m(1+\cos\theta)}{4\pi(H/U_c)(\pi|\underline{x}|/H)^m}\left[i\int_{-\infty}^{\infty}\frac{\exp(-is\Upsilon)(\exp(-sX_+)-\exp(-sX_-))}{(1+iM_c f(sU_c/H)/\pi)}\right]ds+c.c. \tag{2.31}$$

The asymptotic form of the Hankel functions has been used (Abramowitz and Stegun 1964, p364). In (2.31) we have introduced M_c, θ and Υ;

$$M_c = U_c/c, \quad \theta = \arccos(x_1/|\underline{x}|) , \quad \Upsilon = U_c[t]/H, \tag{2.32a}$$

where since $M^2 << 1$

$$[t] = t-t_0-|\underline{x}|/c + Mx_1/c = t-t_0-|\underline{x}|/c(1+M\cos(\theta)). \tag{2.32b}$$

f is defined by (2.21b). Owing to the exponential decay, the major contribution to the integral in (2.31) is from $s << 1/X_+$, where X_+ is the minimum distance of the vortex from the plate as a fraction of the duct height. Correct to neglect of terms of order $(Ms)^2\ln(Ms)$ we find after some calculation and use of Gradshteyn and Ryzhik (1980, p573) that

$$B(\underline{x},t) = A_m(F(\Upsilon,X_+)-F(\Upsilon,X_-)) , \tag{2.33}$$

$$A_m = \frac{(1-V/U_c)(\gamma/2\pi)M_c^m(1+\cos\theta)}{(\pi|\underline{x}|/H)^m(H/U_c)} .$$

Here

$$F(t,x) = \frac{t}{x^2+t^2} - \frac{M_c}{\pi}\frac{d}{dt}\left[\frac{xg(t,x)-t\ln(M_c/2\pi(x^2+t^2)^{1/2})}{x^2+t^2}\right], \qquad (2.34a)$$

and

$$g(x,t) = \pi/2 - \arccos(x/(x^2+t^2)^{1/2}). \qquad (2.34b)$$

Since Y and $X_\pm$ are non-dimensional variables, so is F in (2.33) and A_R is of order uU, where u is the characteristic particle velocity of the vortex. The parameter $Y = U_c[t]/H$ is the retarded streamwise position of the vortex as a fraction of the duct height. The term $F(Y,X_+)$ arises from diffraction by the plate and dominates the term $F(Y,X_-)$ (due to the presence of the wall at $x_2 = 0$) when the vortex passes close to the plate. B/A_R describes the dependence of the far-field enthalpy on the retarded vortex positon. As $|Y| \to \infty$ and the vortex is far from the leading edge the enthalpy decays with $B/A_R \simeq (4h/H)/|Y|^3$. Since (c.f(2.34a))

$$F(t,x) \simeq (t(1+M_c/\pi)-M_c[1+\ln(2\pi x^2/M_c)]/\pi)/x^2 , \quad t \ll x,$$

when $U_c[t] \ll |H-h|$ and the vortex approaches its minimum distance from the plate edge, B/A_R becomes small with

$$B/A_R \simeq (O(U_c[t]/|H-h|)+O(M))/|1-h/H|.$$

B/A_R will have a maximum/minimum when the vortex is respectively downstream/upstream of the plate edge and for $M \ll 1$, $|1-h/H| \ll 1$ this occurs at $Y = \pm|1-h/H|$ where $B/A_R = \pm 1/2|1-h/H|$. Note that the assumption that the vortex convects approximately at the mean flow velocity relies on the assumption Y/H, $Y/|H-h| \ll U$, so that the self-

induced motion of the vortex is negligible. Consequently the results presented here are not valid as $h \to 0$ for fixed Y and U.

The characteristics of B/A_R discussed above are evident in figure 4(a,b) where respectively $M_c = .1,\ .001$ and B/A_R is plotted as a function of $Y = U_c(t)/H$, $|Y| < 1$, for various values of h/H. Figure 4(a) shows that it makes little difference whether the vortex passes above or below the plate though the amplitude $|B/A_R|$ is slightly greater in the former case. Figure 4(b) indicates that for $M_c \ll 1$, $|B|$ does not depend on whether the retarded vortex position is upstream or downstream of the duct mouth. B/A_R is plotted, again as a function of Y in figure 5 for fixed $h/H = .9$ and $M_c = .001,\ .1,\ .2$. Varying the Mach number has little effect save for Y in the region of $-|1-h/H|$.

(i) The far-field within the duct

In the far-field within the duct $\alpha(\underline{x},\omega)$ is given by (A2.36) of Appendix A2 and substitution for α in (2.29), neglect of terms of order $(\omega H/c)^2 \ln(\omega H/c)$ leads to the following expression for $B(\underline{x},t)$;

$$B(\underline{x},t) = A_D\{P(Y,X_+)-P(Y,X_-)\}\ , \qquad (2.35)$$

$$A_D = (1-V/U_c)(\gamma/2\pi)(\pi/2)^{\frac{1}{2}}U_c/H\ ,$$

where

$$P(t,x) = P_+(t,x)-\mathrm{sgn}(t)P_-(t,x)\ ,$$

$$P_\pm(t,x) = q_\pm(t,x)+\frac{M_c}{\pi}\int_{-\infty}^{t} q_\pm(t,x)\left[\ln\left(M_c/8\pi(x^2+t^2)^{\frac{1}{2}}\right)\pm g(t,x)\right]dt\ ,$$

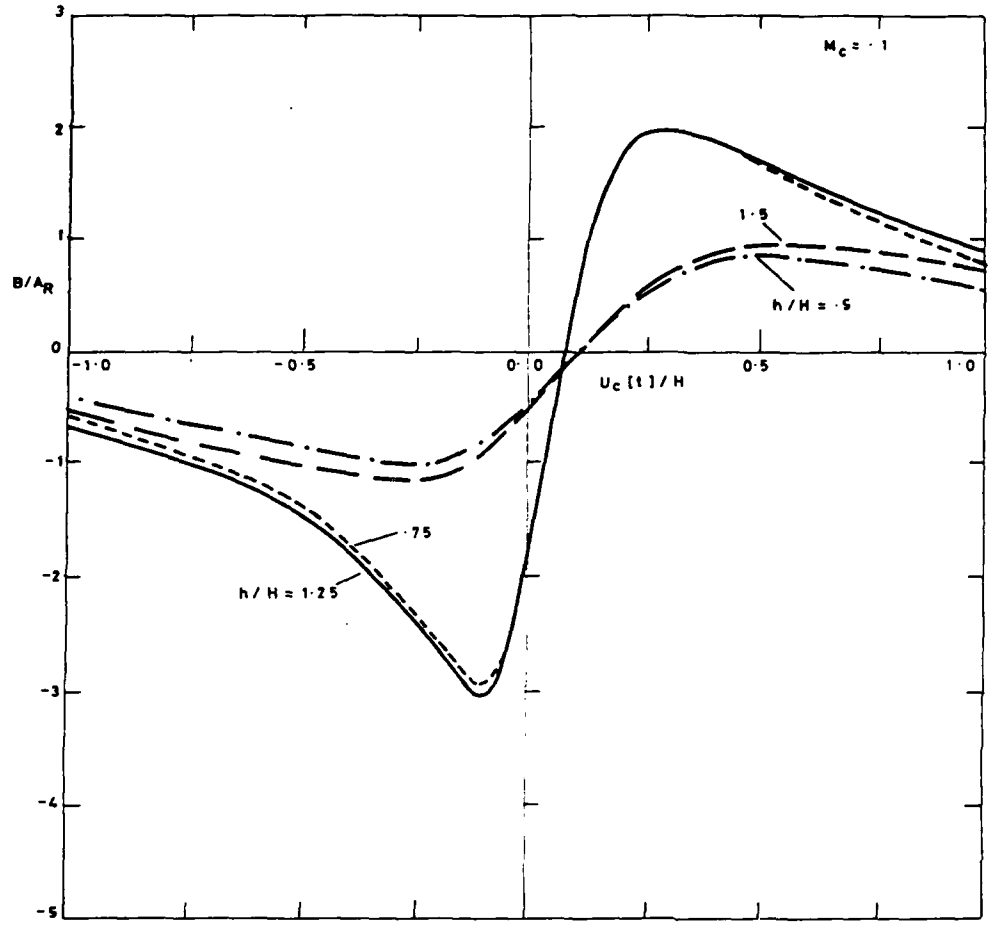

Fig. 4a

Figure 4. B/A_R of (2.33) as a function of $U_c[t]/H$. h/H is as indicated on each curve and (a) $M_c = .1$; (b) .001.

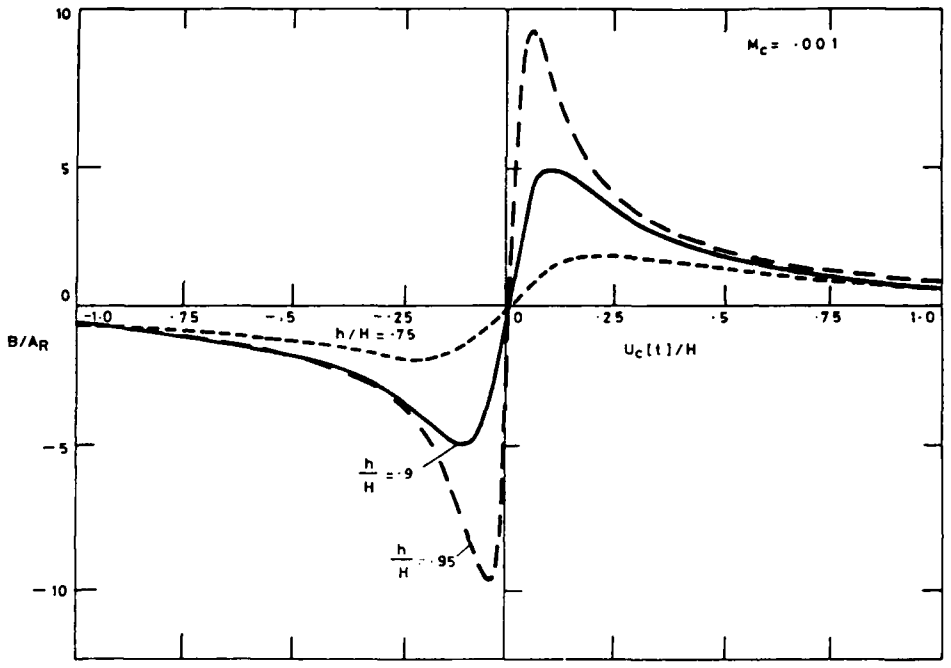

FIG. 4 (b)

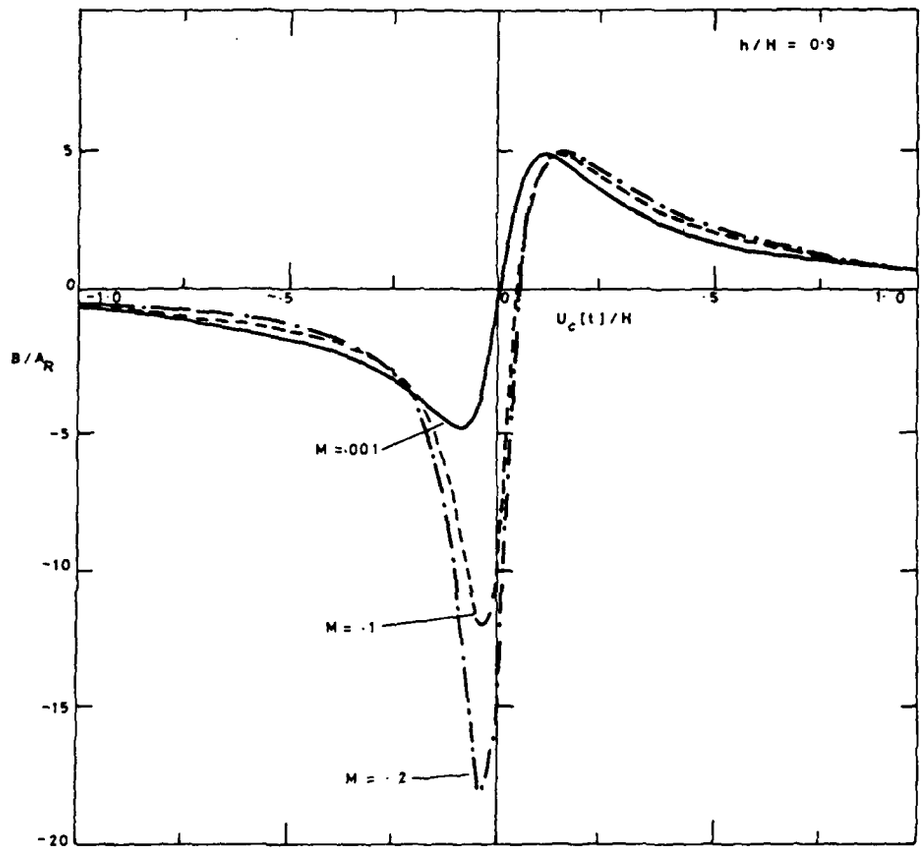

Figure 5. B/A_R of (2.33) plotted against $U_c[t]/H$ for h/H =.9 and M_c = .001, .1, .2 as indicated on each curve.

and

$$q_{\pm}(t,x) = [((x^2+t^2)^{1/2}\pm x)/(x^2+t^2)]^{1/2} , \qquad (2.36a\text{-}c)$$

(c.f. Gradshteyn and Ryzhik 1980, p484 and p574). g is defined by (2.34b). Examination of (2.35) and (2.36) shows that when Y is large and negative (the vortex is far upstream) the field in the duct is small with $B \simeq A_D 2/|Y|^{1/2}$ while when the vortex is far downstream of the edge $B \simeq -A_D 2(h/H)/|Y|^{3/2}$, $h<H$ and $B \simeq -A_D 2/|Y|^{3/2}$, $h > H$. When the vortex approaches its minimum distance from the plate, $U_c[t]/H << |H-h|$, we find for $M_c << 1$

$$B/A_D \simeq 2[(1/|1-h/H|^{1/2})-(1/(1+h/H)^{1/2}] ,$$

and B/A_D has a maximum. This can be seen in figure 6 which shows B/A_D as a function of $U_c[t]/H$ for $M_c = .1$ and various values of h/H. As for the radiated far-field, |B| is slightly greater when the vortex passes above rather than below the plate. The influence of M_c on B/A_D is shown in figure 7 where $h/H=.9$ and $M_c = .01,.1,.2$.

In figure 8 the dependence of the radiated and duct far-field stagnation enthalpies on $U_c[t]/H$ (respectively B/A_R of (2.33) and B/A_D of (2.35)) is compared. Two values of h/H, .5 and .75, are shown and $M_c = .1$. The difference in the two is most apparent at $U_c[t]/H \simeq |1-h/H|$.

§2.6 Harmonic Gust

An incompressible velocity perturbation $\underline{u} = (u_1, u_2)$ of a convected two dimensional gust is

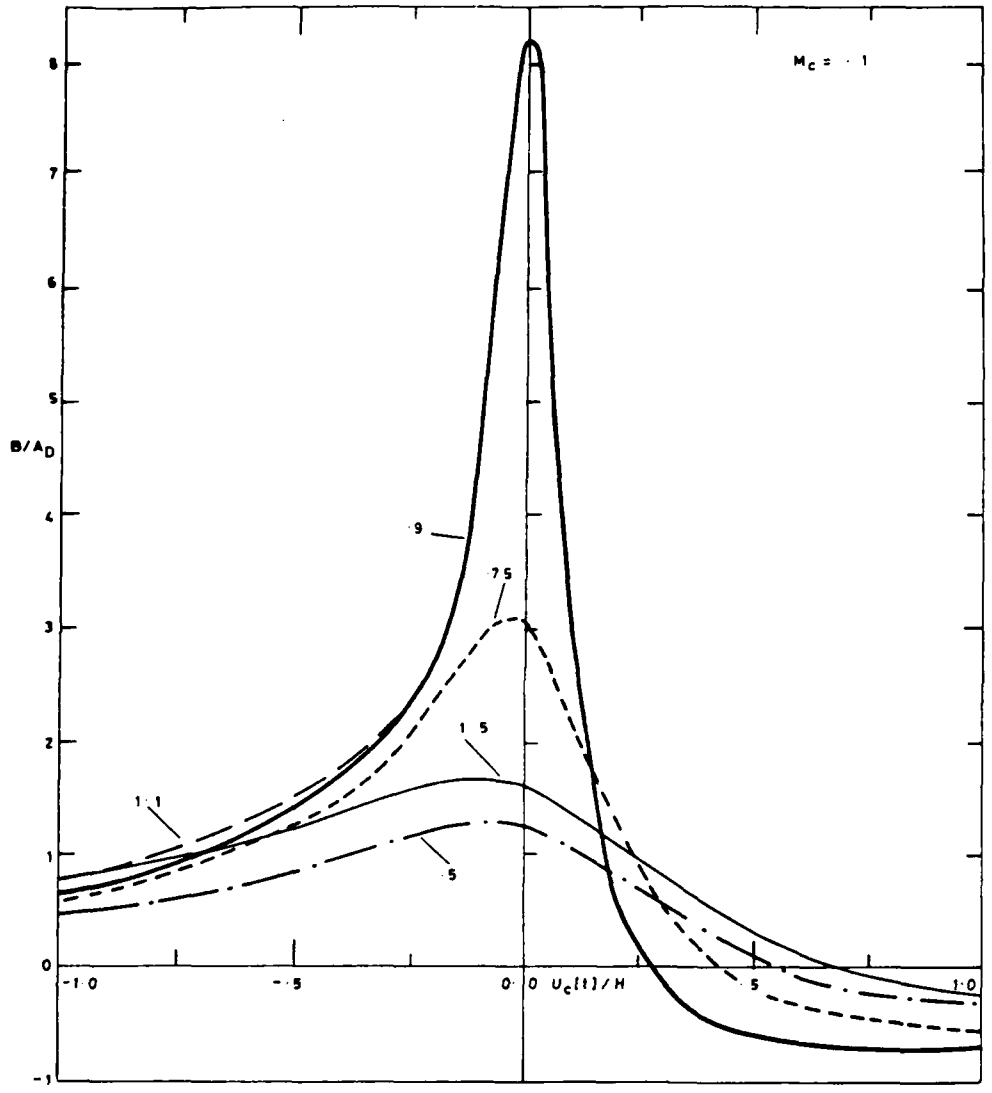

Figure 6. B/A_D of (2.35) as a function of $U_c[t]/H$ with $M_c = .1$ and values of h/H as indicated on each curve.

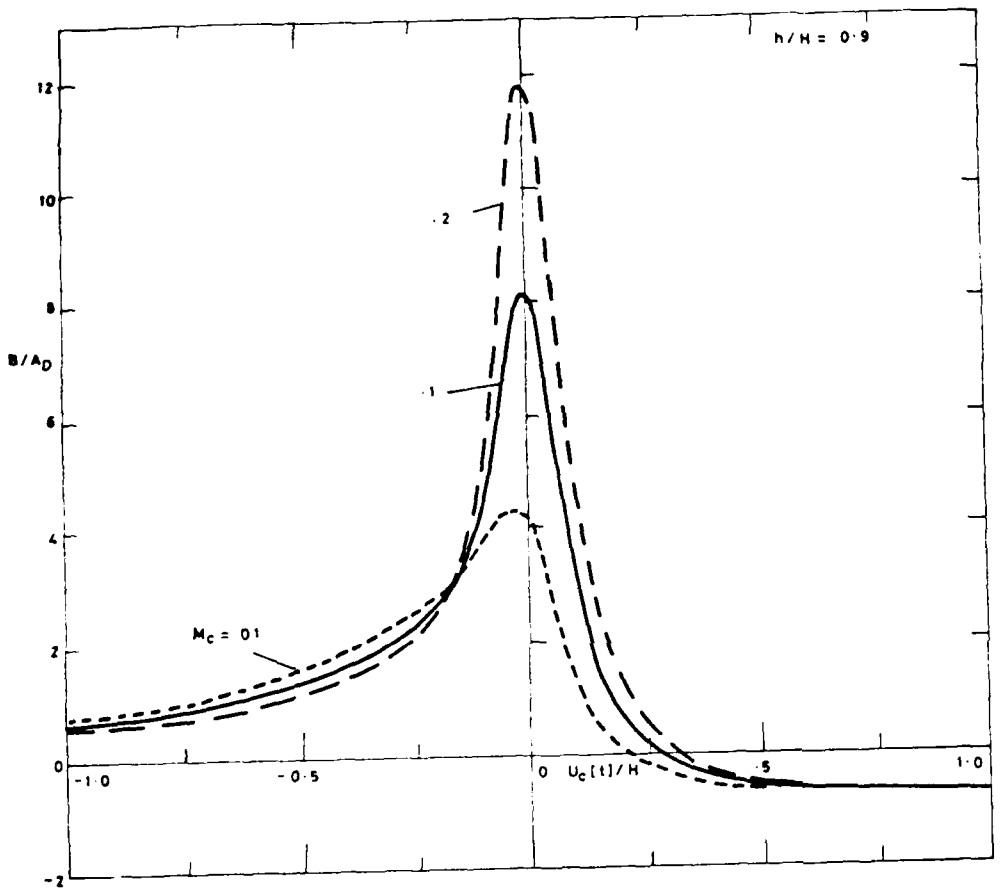

Figure 7. B/A_0 of(2.35) plotted against $U_c[t]/H$ for $h/H = .9$ and $M_c = .01, .1, .2$.

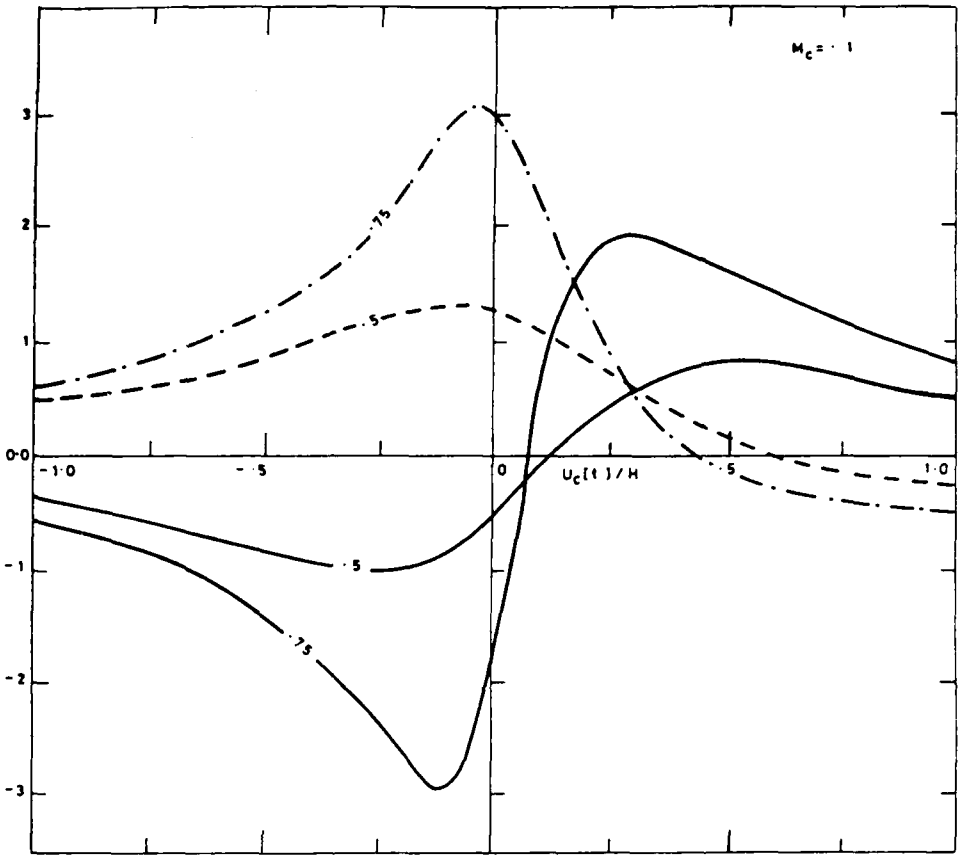

Figure 8. Comparison of B/A_m of (2.33) (solid curves) and B/A_D of (2.35) (dashed curves) with M_c=.1 and h/H = .5, .75 as indicated on each curve.

$$\underline{u} = (C(\underline{K})/K_1)(-K_2,K_1)\exp(iK_1(x_1-U_c t)+iK_2x_2), \qquad (2.37)$$

where $C(\underline{K})$ is a function of the wave-number $\underline{K} = (K_1,K_2)$. In the coordinate system of figure 1 the vorticity of the gust is $\tau\underline{e}$ ($\underline{e}$ is a unit vector out of the plane of the paper) and

$$\tau = (C(\underline{K})(K_1^2+K_2^2)/K_1)\exp(iK_1(x_1-U_c t)+iK_2x_2)\ , \qquad (2.38)$$

$$= (C(\underline{K})(K_1^2+K_2^2)/K_1)\int_0^\infty\int_{-\infty}^{\infty}\exp(iK_1X_1+iK_2X_2)\delta(x_1-U_c t-X_1)\delta(x_2-X_2)dX_1dX_2. \qquad (2.39)$$

The far-field stagnation enthalpy produced by the interaction of the gust with the edge $(0,H)$ of the plate can be calculated by use of the results of §2.4 if we set

$$h=X_2, \quad t_o=-X_1/U_c, \qquad (2.40)$$

and

$$Y = (C(\underline{K})(K_1^2+K_2^2)/K_1)\exp(iK_1X_1+iK_2X_2)dX_1dX_2\ . \qquad (2.41)$$

$B(\underline{x})$ is found by integration of the stagnation enthalpy for the line vortex case of §2.4 over the variables X_1, X_2 as in (2.39). In this way we obtain with (2.31)

$$B(\underline{x}) = \frac{C(\underline{K})(1-V/U_c)H^{m}(1-i\,\mathrm{sgn}(K_1))\alpha(x,K_1U_c)\exp(-K_1U_c(t+Mx_1/c))}{2\pi\qquad\qquad |K_1|^{m}}$$

$$\cdot(\exp(iK_2H)-\exp(-|K_1|H)). \qquad (2.42)$$

Result (2.31), used to derive (2.45), is valid for short vortex waves. Thus we require $|K_1 H| >> 1$ and neglect the final term in the curly brackets of (2.45).

(i) Outside the duct, $|x| >> 1/|K_1 H|$

From (2.21) with the asymptotic form of the Hankel functions and (2.42) we find

$$B(x) = \frac{iC(K)(1-V/U_c)(1+\cos\theta)M_c^{m}\,\mathrm{sgn}(K_1)\exp(iK_2 H - iK_1 U_c[t])}{2\pi(\pi|x|/H)^{m}[1+iK_1 M_c H f(K_1 U_c)/\pi]}, \qquad (2.43)$$

where $[t]$ is defined by (2.32) with $t_o = 0$.

(ii) Inside the duct, $|x| >> 1/|K_1 H|$

From (2.45), (A2.36) of Appendix A2 we find for the far-field enthalpy

$$B(x) = \frac{C(K)(1-V/U_c)(1-i\,\mathrm{sgn}(K_1))\exp(iK_2 H - iK_1 U_c[t])}{2\pi(|K_1|H)^{m}[1+iK_1 M_c H f(K_1 U_c)/\pi]}, \qquad (2.44)$$

where $[t]$ is defined by (2.32b) with $t_o = 0$ and $\theta = 0$.

§2.7 Acoustic energy flux

The flux of acoustic energy (the Blokhintzev definition, c.f. Blokhintzev 1946) through a surface S is ∏ say, where

$$\Pi = \int_S (\rho \underline{v} B + \underline{U} \rho' B) . \underline{n} \, dS \, . \qquad (2.45)$$

ρ, $\underline{U} = (U, 0)$ are respectively the mean density and velocity; the perturbation density, velocity and stagnation enthalpy are ρ', $\underline{v}$ and B. $\underline{n}$ is a unit normal to the surface S. The adiabatic relation between density and pressure and the linearized Bernoulli equation are used in (2.45) to give, neglecting M^2 relative to unity,

$$\Pi = \rho \int_S B(\underline{v} + B\underline{U}/c^2) . \underline{n} \, dS \, . \qquad (2.46)$$

(i) Line vortex

The power flux through the surface S_R of figure 9, a circular arc centred on the origin with radius $R = |\underline{x}| \to \infty$, is Π_R say where

$$\Pi_R = \rho \int_{\theta_0}^{\pi} B(v_n + M(\cos\theta)B/c)|\underline{x}| d\theta \, , \qquad (2.47)$$

and $\theta_0 = \arcsin(H/|\underline{x}|) \to 0$. v_n is the fluid perturbation velocity in the radial direction and is calculated from Bernoulli's equation;

$$\partial v_n/\partial t = -\partial B/\partial |\underline{x}| \, . \qquad (2.48)$$

(2.32) and expression (2.33) for B give, where we now set $U_c = U$,

$$\partial v_n/\partial t = (1/c(1+M\cos(\theta)))\partial B/\partial t \, . \qquad (2.49)$$

Using (2.49) in (2.47) and again neglecting M^2 relative to unity, we find

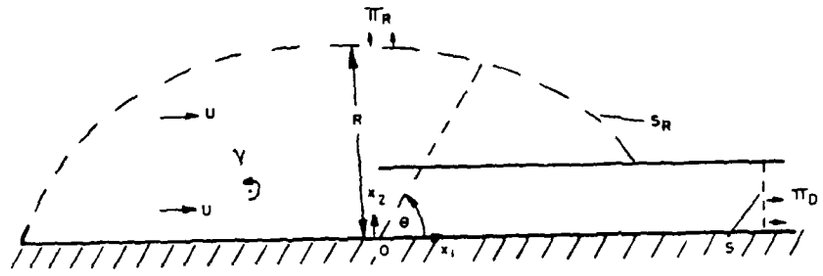

Figure 9. Illustration of the surfaces in the far-field through which the radiated and duct power fluxes are calculated.

$$\Pi_R \simeq (\rho/c)\int_0^{\pi} B^2|\underline{x}|\, d\theta \ ,$$

and with (2.33) this becomes with $U_c = U$,

$$\Pi_R/\Pi = (3(1-V/U)^2M^2/2)[F(U[t]/H,|1-h/H|)-F(U[t]/H,1+h/H)]^2 \ , \quad (2.50)$$

where

$$\Pi = \rho(\gamma/2\pi)^2/(H/U) \ . \quad (2.51)$$

The θ dependence of $[t]$ has been neglected in obtaining (2.50) where now $[t] = t-t_o-|\underline{x}|/c$. The flux through the surface S at $x_1 = \infty$, $x_2<H$, (see figure 9) is Π_D say, and from (2.46), (2.35) we obtain for $M^2<<1$

$$\Pi_D/\Pi \simeq (\pi/2)(1-V/U)^2M|P(U[t]/H,|1-h/H|)-P(U[t]/H,1+h/H)]^2, \quad (2.52)$$

where $[t] = t-t_o-|\underline{x}|/c$.

In figures 10, 11, and 12 the power fluxes, normalised by Π of (2.51) are plotted in dB against $U[t]/H$, $|U[t]/H|<1$, and $V/U = 0.6$. Π_D and Π_R are compared in figure 10(a-c) where $M = .1$ and (a) $|1-h/H| = .25$; (b) .1; (c) .01. Each curve has a singular point because $\Pi_R/\Pi = 0$ where B/A_R of (2.36) is zero and $\log_{10}(\Pi_R/\Pi) \to -\infty$. Similarly $\Pi_D/\Pi = 0$ when B/A_D of (2.35) is zero. Over the range of $U[t]$ shown in the figure we see that the duct power flux is greater than that radiated except for a period in $[t] > 0$ which contains the point $\Pi_D = 0$ (e.g. for $h/H = 1.25$ in figure 10(a), this range is $.31 < U[t]/H < .75$). The difference in the results for the vortex passing above and below the plate (if there is any) is indicated in each of the plots.

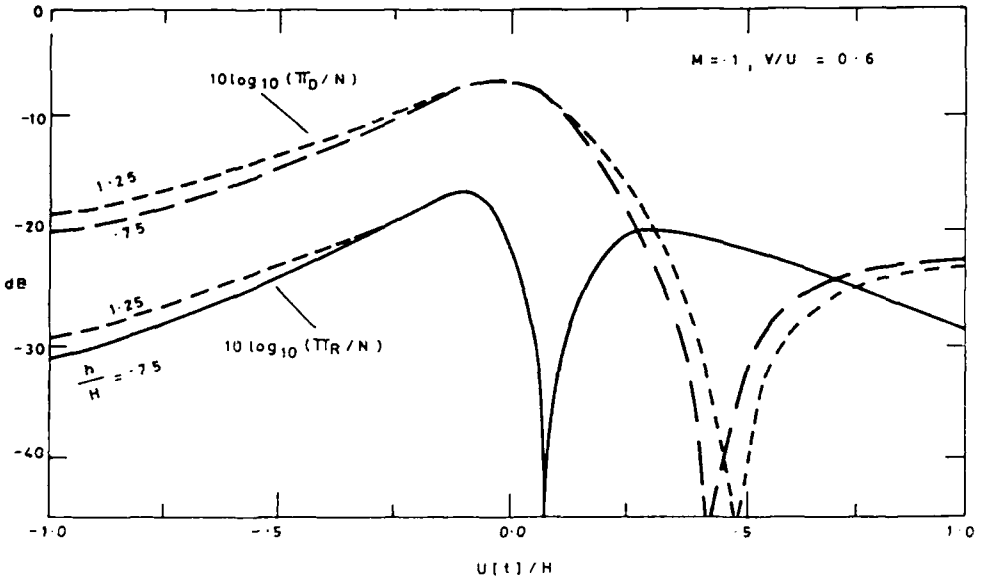

FIG. 10(a)

Figure 10. The normalised power fluxes Π_R/N, Π_D/N of (2.50) and (2.52) respectively, plotted in dB against $U_c[t]/H$ with V/U = .6 and M = .1: (a) |1-h/H|=.25; (b).1; (c) .01.

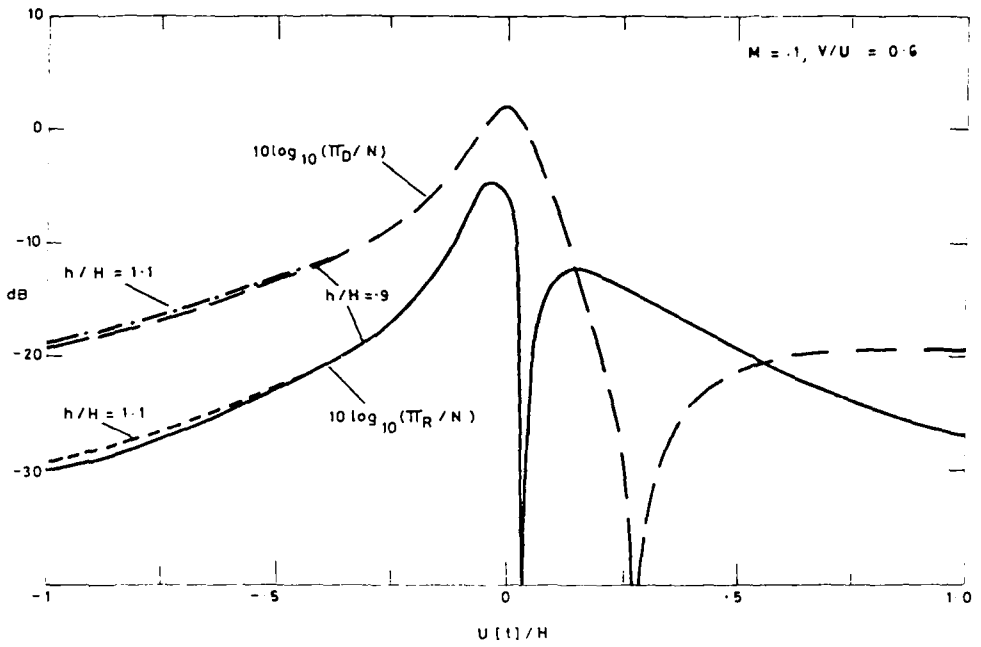
M = ·1, V/U = 0·6
10log10(TTD/N)
h/H = 1·1
h/H = ·9
h/H = 1·1
10 log10(TTR/N)
dB
10
0
-10
-20
-30
-1
-·5
0
·5
1·0
U[t]/H

FIG. 10 (b)

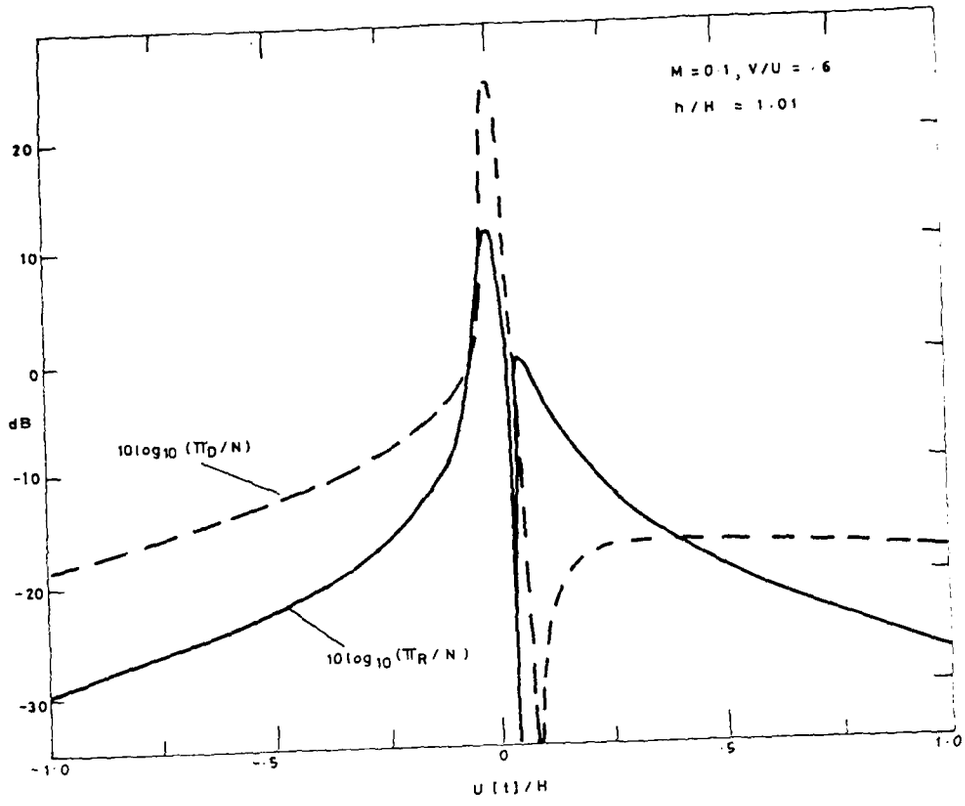
M = 0·1, V/U = ·6
h/H = 1·01
20
10
0
dB
-10
-20
-30
10 log10 (ΠD/N)
10 log10 (ΠR/N)
-1·0
-·5
0
·5
1·0
U[t]/H

FIG. 10 (c)

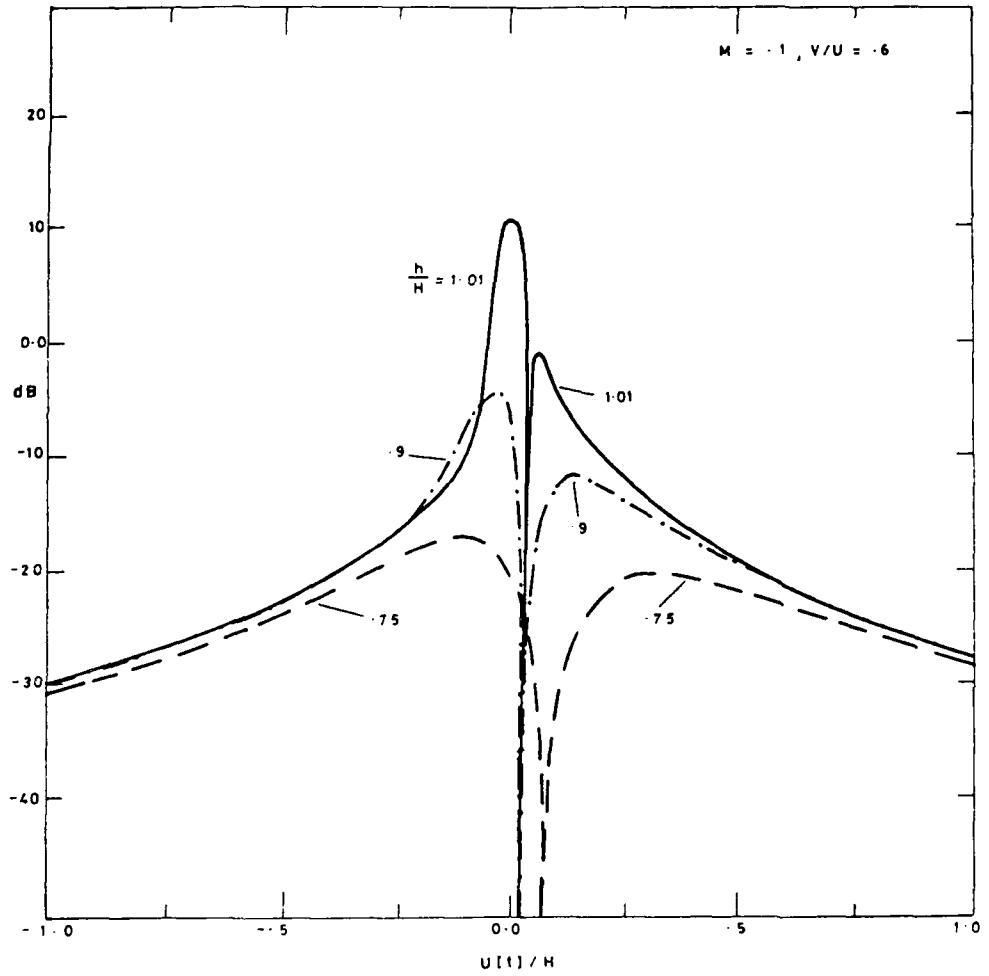

Figure 11. $10\log_{10}(\Pi_M/\Pi)$ of (2.50) as a function of $U_c[t]/H$ with $V/U = .6$, $M=.1$. h/H is indicated on each curve.

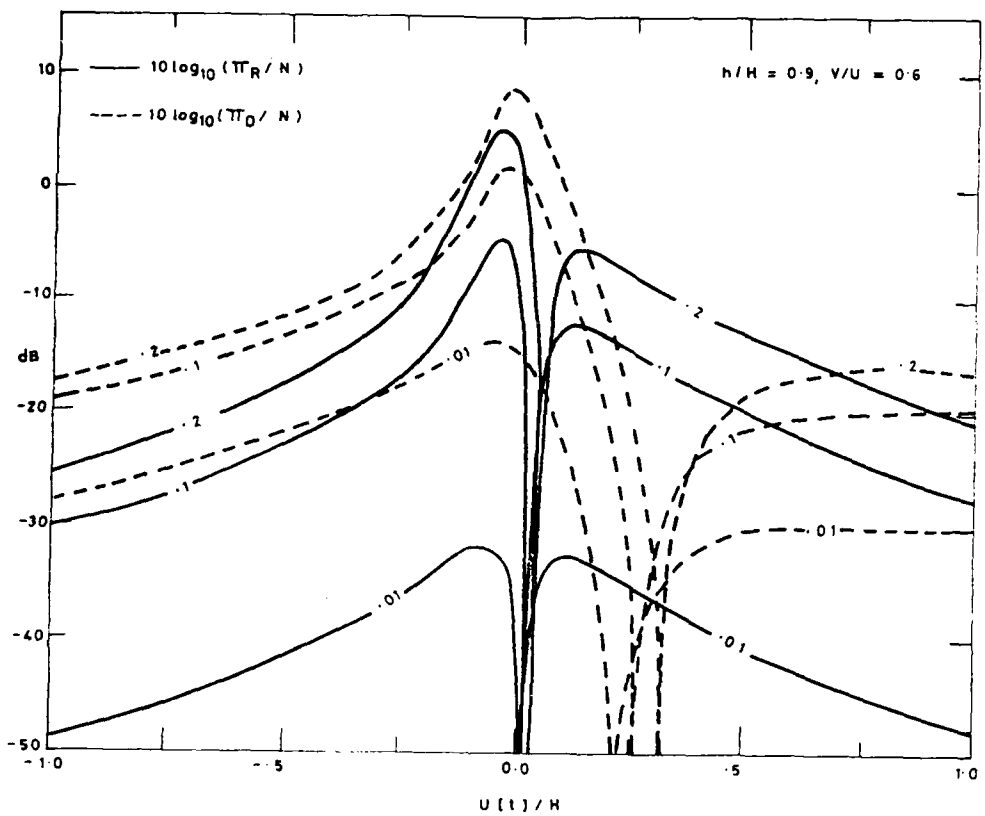

Figure 12. $10\log_{10}(\Pi_R/N)$ (solid curves) and $10\log_{10}(\Pi_D/N)$ (dashed curves) plotted against $U_c[t]/H$ with $V/U = .6$ and $N = .01$, .1, .2, as indicated on each curve.

Figure 11 shows Π_R/Π for different values of h/H and again M=.1. The peak of each curve increases as the minimum distance of the vortex from the plate |H-h| is decreased. Though the functions F and P (respectively of (2.34), (2.36)), appearing in the radiated and duct power fluxes have a Mach number dependence the predominant influence is that Π_R/Π varies as M^2 whereas Π_D/Π is proportional to M. This is illustrated in figure 12 where Π_R/Π (solid lines) and Π_D/Π (dashed lines) are plotted for h/H = .9 and M = .01, .1, .2 as indicated on each curve.

(ii) Harmonic gust

Π_R, Π_D, defined in the preceding section, are respectively the power radiated to the far-field outside the duct and through the duct. In a calculation similar to that described between (2.45) and (2.50) with B now given by (2.43), (2.44) (additionally taking real parts of functions and averaging over a wave period $2\pi/K_1U$) the following are obtained:

$$\Pi_R = \frac{3\rho H|C(\underline{K})|^2(1-V/U)^2M}{16c\pi^2|1+iK_1MHf(K_1U)/\pi|^2} , \qquad (2.53)$$

$$\Pi_D = \frac{\rho H|C(\underline{K})|^2(1-V/U)^2}{2c\pi^2K_1H|1+iK_1MHf(K_1U)/\pi|^2} , \qquad (2.54)$$

and

$$\Pi_T = \Pi_R/\Pi_D = 3M|K_1|H/8 ,$$

$$= 3|\omega|H/8c . \qquad (2.55)$$

where $\omega = K_1U$ is the radian gust frequency.

§3 Plane wave radiation from the duct

§3.1 The far-field potential

The radiation of a plane wave, $\phi_i \exp(-i\omega t)$, from the semi-infinite duct formed by the plate and wall is now discussed (see figure 13). The incident plane wave is given by

$$\phi_i = \phi_o \exp(-i\omega k_o x_1/(1-M)) \ , \ k_o = \omega/c \ , \qquad (3.1)$$

and propagates upstream from within the duct. ϕ_o is a constant and flow quantities, such as M, ρ and c are as described in §2.

The total perturbation potential, $\phi\exp(-i\omega t)$ say, is the solution of the convected wave equation ((2.2) with the right hand side replaced by zero) which satisfies the boundary conditions

$$\partial\phi/\partial x_2 = \begin{cases} \nu(\omega)\exp(i\chi x_1) \ , & x_1 > 0, \ x_2 = H\pm 0, \\ \\ 0 \ , & x_2 = 0, \ |x_1| < \infty \ , \end{cases} \qquad (3.2)$$

and

$$\phi \to \text{constant}.\exp(ik_o|\underline{x}|/(1+M\cos(\theta))/|\underline{x}|^m \ , \ |\underline{x}| \to \infty \ , \qquad (3.3)$$

$$\theta = \arccos(x_1/|\underline{x}|),$$

for $\underline{x}$ outside the duct. ϕ and $\partial\phi/\partial x_2$ must also be continuous on $x_1 < 0$, $x_2 = H$. The boundary conditions in (3.2) are the same as those for the vortex which are dicussed in §2.2. The Prandtl-Glauert

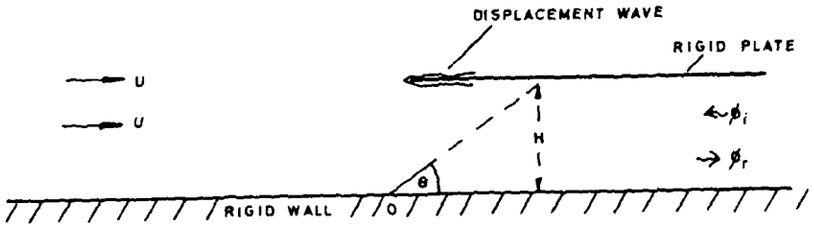

Figure 13. Radiation of a plane wave from the duct.

transform of (2.9) is employed again with $\tilde{\phi}$ denoting the transform of ϕ and $\tilde{\phi}_i$ that of ϕ_i where

$$\tilde{\phi}_i = \phi_o \exp(-ik_o x_1) \ . \tag{3.4}$$

With the Green's function of equation (2.11) we find on application of the Divergence theorem to the fluid in the region V sketched in figure 3 that

$$\tilde{\phi}(\underline{x}) = -\int_S \{ G(\underline{x};\underline{y})\nabla\phi(\underline{y}) - \phi(\underline{y})\nabla G(\underline{x};\underline{y}) \}. \ \underline{n} \ dS \ , \tag{3.5}$$

where S, the boundary of V is as described in §2.3 and sketched in figure 3. The radiation conditions satisfied by G and ϕ ensure that the portion of the surface integral over S_R, the circular part of S, is zero and that only the component $\tilde{\phi}_i$ of $\tilde{\phi}$ contributes to the integral over the surface $y_1 = \infty$, $|y_2| < H$. On applying the condition (3.2) we obtain with (A2.4) of Appendix A2

$$\phi(\underline{x}) = -\nu(\omega)\int_o^\infty [G(\underline{x};\underline{y})]^+ \exp(i\chi y_1) \ dy_1 \ - \phi_o 2ik_o HA(\underline{x},\omega). \tag{3.6}$$

The notation $[f]^+$ is explained by (2.6) and $G(x;y) \to A(\underline{x},\omega)\exp(ik_o y_1)$, $y_1 \to \infty$ defines A, which is calculated in Appendix A2. The integral on the right hand side of (3.6) arises from the presence of displacement waves on the plate boundary layers. We assume that since the displacement waves must decay or become incoherent as they propagate downstream the major contribution to the integral comes from the region $y_1 << 1/\chi$, and the integral is evaluated by use of the

approximation (2.20a), $[G]^{+}_{-} = \alpha[\phi]^{+}_{-}$, which is valid for $|\underline{x}|$ within an acoustic wavelength of the plate edge, $|\underline{x}|$ in the far-field. On the assumption of short displacement waves, $\chi H >> 1$, a further approximation for $[\phi]$ given by (A1.11) can be used in (3.6) and with result (2.24) we find on reverting to the actual potential ϕ (c.f. (2.9))

$$\phi(\underline{x}) = -\exp(-ik_0 M x_1)\left[\frac{\alpha(\underline{x},\omega)\psi(\omega)(H/|\chi|)^{m}(1-i)}{|\chi|} + \phi_0 2ik_0 H A(\underline{x},\omega)\right]. \tag{3.7}$$

$\psi(\omega)$ is determined by the Kutta condition in Appendix A4, (A4.16) and α, A are given respectively in equations (A2.12), (A2.13) of Appendix A2 for $\underline{x}$ in the far-field outside the duct and by (A2.17), (A2.14) when $\underline{x}$ is far downstream within the duct.

Substitution for $\psi(\omega)$ gives

$$\phi(\underline{x}) = -k_0 H \phi_0 \exp(-ik_0 M x_1)\{ ([1-R+M(1+R)]\alpha(\underline{x},\omega)/\chi) + 2iA(\underline{x},\omega)) . \tag{3.8}$$

R is a reflection coefficient when $\phi = \phi_d$, the perturbation potential in the absence of displacement waves and is defined by

$$\phi_d(\underline{x}) \to \phi_i(\underline{x}) + \phi_r(\underline{x}) , \quad x_1 \to \infty, \quad |x_2| < H, \tag{3.9}$$

$$\phi_r(\underline{x}) = \phi_0 R \exp(ik_0 x_1/(1+M)) .$$

R is determined from (3.7) by setting $\psi(\omega) = 0$ and use of results (A2.14), (A2.15) of Appendix A2. Then comparison with (3.9) gives

$$R = -\left[\frac{1 - i\omega Hf(\omega)/\pi c}{1 + i\omega Hf(\omega)/\pi c}\right], \tag{3.10}$$

where $f(\omega)$ is defined in (2.21b).

(i) The radiated field

As in (2.7) we set $\chi = \omega/V$. Results (A2.8a,b), (A2.12), (A2.13) of Appendix A2, in which the asymptotic form of the Hankel functions (Abramowitz and Stegun 1964, p364) are substituted, give with (3.8) and (3.10) for $\omega|x|/c \to \infty$

$$\phi(\underline{x})\exp(-i\omega t) \to \frac{-\phi_o(1-i)(\omega H/\pi c)^{\frac{1}{2}}}{(|x|/H)^{\frac{1}{2}}}\left[\frac{1-(i\omega Hf(\omega)\cos\theta/\pi c)+\epsilon(1+\cos\theta)}{[1+i\omega Hf(\omega)/\pi c]}\right]\exp(-i\omega[t]), \tag{3.11}$$

$$\epsilon = (V/U)M\left[\frac{1+i\omega HMf(\omega)/\pi c}{1+i\omega Hf(\omega)/\pi c}\right], \tag{3.12}$$

where $[t] = t-|x|/(c(1+M\cos\theta))$, correct to neglect of terms of order M^2 relative to unity. The far-field pressure, $p\exp(-i\omega t)$, is found from the linearized Bernoulli equation which gives, again neglecting M^2 relative to unity, $p/\rho = i\omega(1-M\cos\theta)\phi$.

The intensity of the radiated sound, averaged over a wave period $2\pi/\omega$, is $|p|^2/2\rho c$ and from (3.11) we find

$$\frac{|p|^2}{2\rho c} = \left\{\frac{|p_i|^2}{2\rho c}\right\} \frac{2(1-M)^2 k_o H\, D_R}{(\pi|x|/H)}, \quad \omega|x|/c \gg 1, \tag{3.13}$$

where D_R is a directivity factor defined by

$$D_R = (1-M\cos\theta)^2 \left| \frac{1-(i\omega H f(\omega)(\cos\theta)/\pi c)+\epsilon(1+\cos\theta)}{1 + i\omega H f(\omega)/\pi c} \right|^2, \tag{3.14}$$

and

$$|p_i|^2/2\rho c = \rho(\omega|\phi_o|/(1-M))^2/2c \tag{3.15}$$

is the intensity of the incident wave ϕ_i of (3.1). In the long wavelength limit we find, neglecting of terms of order $(\omega H/c)^2$ relative to unity

$$D_R = (1-M\cos\theta)^2\{1-(1+\cos\theta)[k_o H-(V/U)M(2-k_o H(3+\cos\theta))]\}, \tag{3.16}$$

$$\omega H/c \ll 1.$$

The term involving V/U in (3.15) is the change in the far-field intensity from that of the 'no displacement wave case' and indicates that for long sound wavelength the intensity is increased by an amount which is proportional to VM/U.

The directivity factor D_R is plotted against θ° in figure 14 for various values of $k_o H$, V/U = .6 and (a) M = .1; (b) M= .01. The maximum is at $\theta = 180^\circ$, upstream of the duct on the wall at $x_2 = 0$, when $D_R = (1+M)^2$. The minimum attained by D_R depends on $k_o H$, decreases as $k_o H$ increases and occurs for $k_o H \leq 1$ at 0°. The results presented here are strictly valid only for low frequencies, certainly

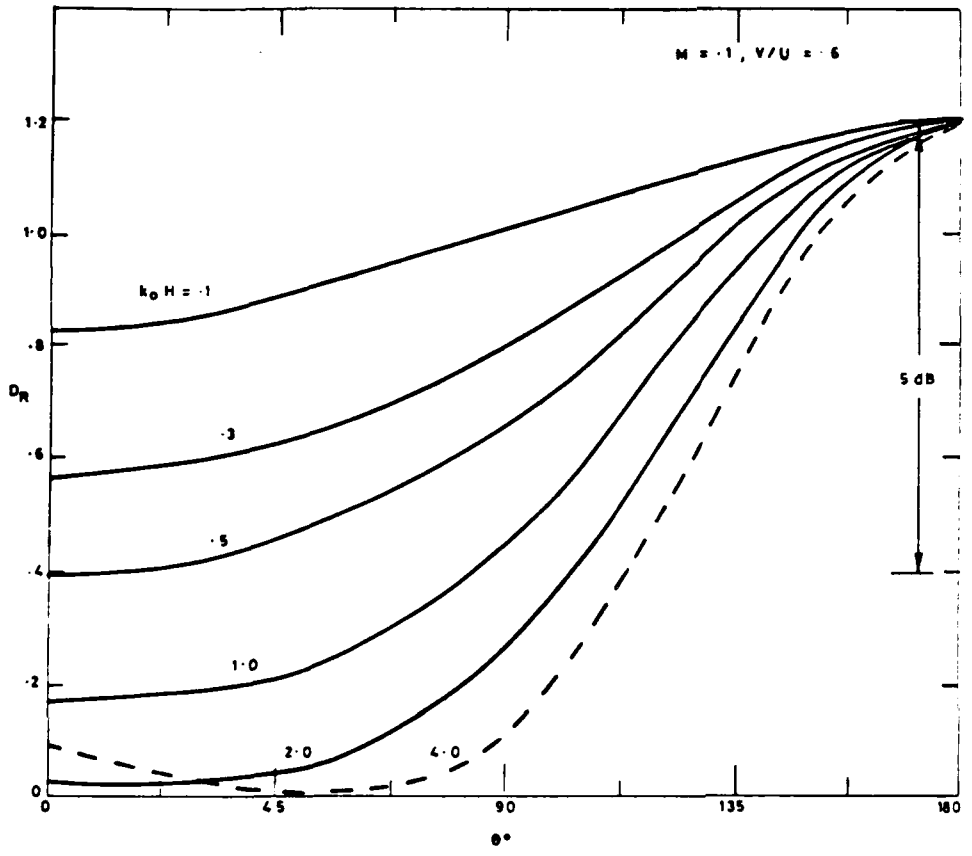

FIG. 14 (a)

Figure 14. The directivity factor of the far-field pressure, D_R of (3.16), as a function of θ, with V/U = .6 and (a) M=.1; (b) .01. The value of k_0H is indicated on each curve.

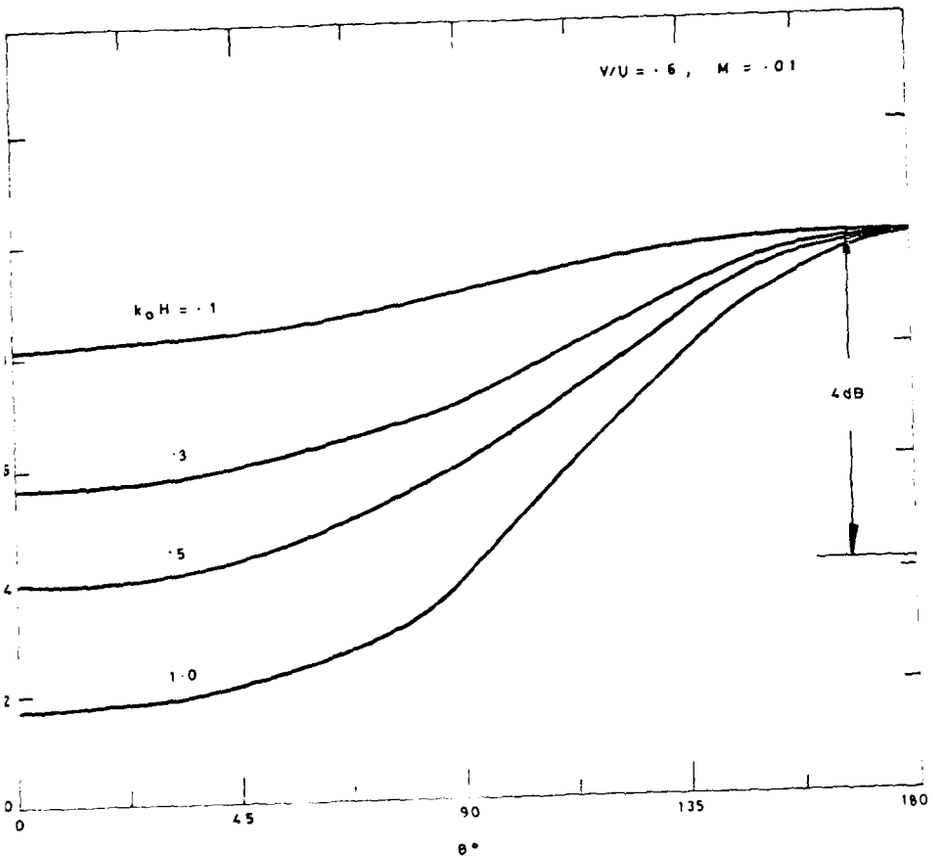

FIG. 14 (b)

below the cut-off of transverse duct modes, i.e $k_oH < \pi/2$, but results are shown for greater values of k_oH. The figure reveals that D_R can become very small for values of $k_oH > 1$ and θ close to 0°. Figure 14(b) shows that between the upstream and downstream directions there is a difference of 4 dB at $k_oH = .5$.

(ii) The duct field

The far-field potential within the duct can be expressed as

$$\phi(\underline{x}) = \phi_i(\underline{x}) + \phi_d(\underline{x}) + \phi_b(\underline{x}) , \qquad (3.17)$$

where $\phi_b(\underline{x})$ is a reflected wave arising from the presence of displacement waves on the plate and $\phi_d(\underline{x})$ is the reflected field in their absence given by (3.9), (3.10). The total reflected field, $\phi_r(\underline{x})+\phi_b(\underline{x})$ can be written as a single reflected wave with reflection coefficient $\bar{R}$;

$$\phi_r(\underline{x})+\phi_b(\underline{x}) = \phi_o\bar{R}\exp(ik_ox1/(1+M)) , \qquad (3.18)$$

and from (3.8)-(3.10)

$$\bar{R} = -\frac{(1 - (ik_oHf(\omega)/\pi) + 2\epsilon)}{(1 + ik_oHf(\omega)/\pi)} . \qquad (3.19)$$

In the absence of displacement waves $\epsilon = 0$ and then in the long wavelength limit $\bar{R} \to -1$. In terms of pressure amplitudes with p_i that of the incident wave and p_r that of the reflected field of (3.18) we find

$$|p_r|/|p_i| = ((1-M)/(1+M))|\bar{R}| \quad . \tag{3.20}$$

Experiments have been conducted at the Institute of Sound and Vibration Research of Southampton university to measure the field reflected at the mouth of an open pipe which has a low mean flow Mach number inflow and white noise excitation within the pipe, downstream of the mouth (Davies 1987). Comparison with the present theory is possible only on a qualitative level since in the experiments the geometry is that of a circular pipe, rather than a two-dimensional duct; the inflow is produced by suction within the pipe and is consequently non-uniform around the mouth. Also the theory assumes that the flow does not separate at the duct mouth whereas for a sharp pipe entry the experimental flow consisted of a shear layer of thickness around .2a (a is the pipe radius). A bell mouthed pipe entry, also examined in the experiments, had smooth entry flow but its pipe wall (of radius of order a at the mouth) does not resemble the thin wall discussed here. Nevertheless in the latter case the measurements of the ratio of equation (3.20), normalized by its no-flow value are curve fitted by $[(1-M)/(1+M)]^{.9}$ which Davies points out is greater than the value $[(1-M)/(1+M)]$ which a potential flow solution would predict. The presence of coupled instability waves in the pipe boundary layers is suggested as the cause of the enhanced reflected wave amplitude. This explanation is in accord with the present analysis which from (3.12), (3.19), (3.20) gives the ratio as

$$\frac{(1-M)[1+2(V'/U)M]}{(1+M)} = [(1-M)/(1+M)]^{(1-V'/U)} \quad ,$$

(M^2 and $(k_oH)^2$ are neglected relative to unity). This prediction of the ratio is, for V/U = .6, much greater than that of the experiment but shows that flow/acoustic interaction at the duct mouth can explain the increase in the reflected field.

3.2 Acoustic energy

Equation (2.45) gives the instantaneous acoustic energy flux through a surface S. Here we discuss the time-averaged, i.e. averaged over a wave period $2\pi/\omega$, power flux away from the plate leading edge. The flow of acoustic energy through the surface S, sketched in figure 9 and defined by $x_1 = L >> c/\omega$, $|x_2| < H$, is $\overline{\Pi}_D$. The perturbation field at S is given by equations (3.17)-(3.19). Restoring the time factor $\exp(-i\omega t)$, taking real parts of functions and averaging, yields

$$\overline{\Pi}_D = - \overline{\Pi}_i(1-|\bar{R}|^2), \tag{3.21}$$

where $\overline{\Pi}_i$ is the power flux of the incident wave ϕ_i of (3.1) and

$$\overline{\Pi}_i = \rho\omega|\phi_o|^2 k_oH/2 \ . \tag{3.22}$$

Calculation of $|\bar{R}|^2$ from (3.19) correct to second order in k_oH shows that

$$\overline{\Pi}_D/\overline{\Pi}_i \simeq -2k_oH(1-k_oH - 2(V/U)M(1-2k_oH)/k_oH) \ , \ k_oH << 1. \tag{3.23}$$

The time-averaged flux through S_∞ of figure 9 (a circular arc centred on the origin with $k_o|x| >> 1$) $\overline{\Pi}_\infty$ say, is found in a similar manner using (3.11) and (3.12);

$$\Pi_R/\Pi_i = \frac{2k_oH\ (\ |1+\epsilon|^2 + |\epsilon - ik_oHf(\omega)/\pi|^2/2\ )}{|\ 1 + ik_oHf(\omega)/\pi|^2}\ , \qquad (3.24)$$

where ϵ is defined by (3.12) and f by (2.21b). In the limit $k_oH \to 0$, neglecting M^2 relative to unity, this becomes

$$\Pi_R/\Pi_i \to 2k_oH\ (\ 1-k_oH + 2M(V/U)\ )\ . \qquad (3.25)$$

In the long wavelength limit the net flux of acoustic energy away from the plate edge is from (3.23) and (3.25)

$$\Pi_R + \Pi_D \simeq \Pi_i 4M(V/U)(\ 1-k_oH\ )\ ,\ k_oH \ll 1. \qquad (3.26)$$

Acoustic energy is not conserved due to the presence of displacement waves on the plate boundary layers and (3.26) shows that for low frequencies the total flux away from the plate is positive; sound energy is produced by the flow acoustic/interaction at the plate edge.

In figure 15 the radiated and duct energy fluxes normalized by Π_i and respectively of (3.21), (3.24), are plotted in dB against k_oH for $V/U = .6$. Also shown is a transmission factor $\Pi_T = \Pi_R/|\Pi_{Do}|$, which is the radiated power as a fraction of the duct power flux. Though the results are valid only for $k_oH \ll \pi/2$ a much greater range is shown in figure 15(a) where $M = .1$. A more detailed picture of these results for $k_oH < 1$ is given in figure 15(b). Singular points in the curves for Π_D and Π_T are evident at $k_oH \simeq .1$. This is where $|R|^2 = 1$ in (3.21) and $\Pi_D = 0$. For $k_oH < .1$ the net duct energy flux is positive in the direction of the reflected field, i.e. in the

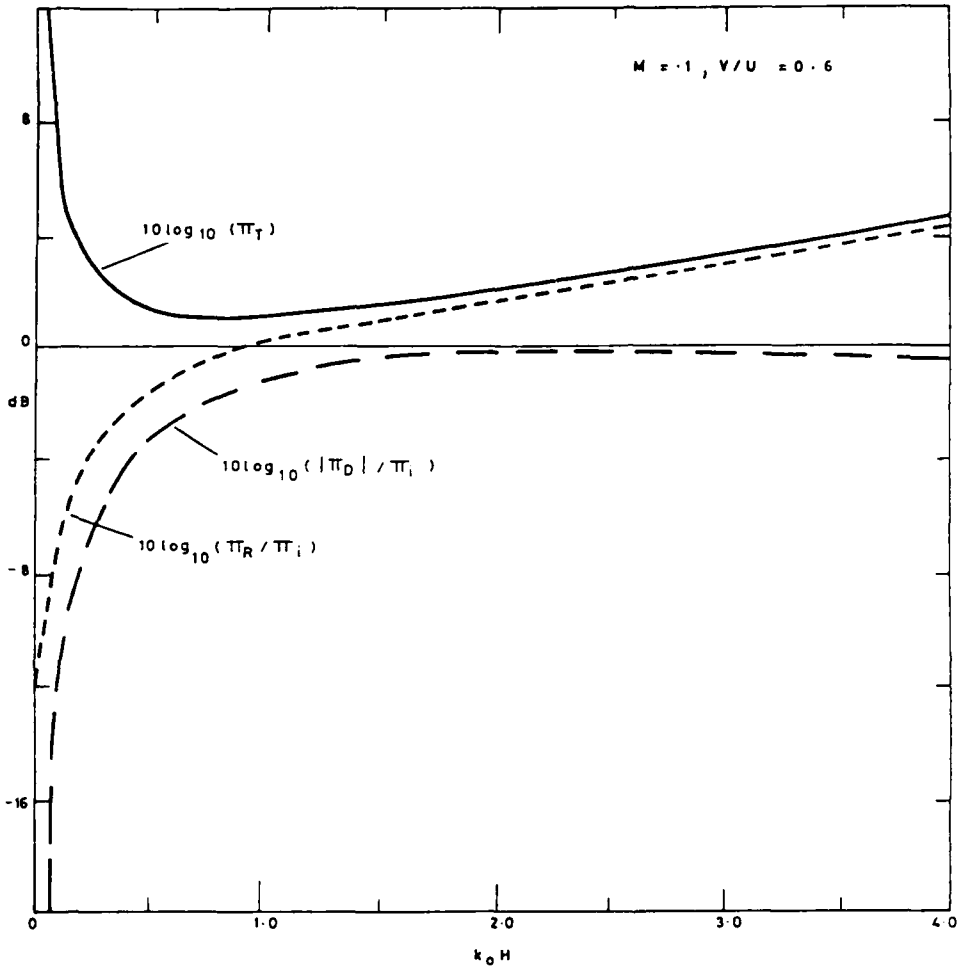

FIG. 15 (a)

Figure 15. The normalized radiated and duct power fluxes, Π_R and Π_D of (3.21), (3.24) respectively, plotted in dB against k_0H with V/U = .6 and (a) M = .1, $k_0H \leq 4.$; (b) M = .1, $k_0H \leq 1.$; (c) M = .01, $k_0H \leq 1.$

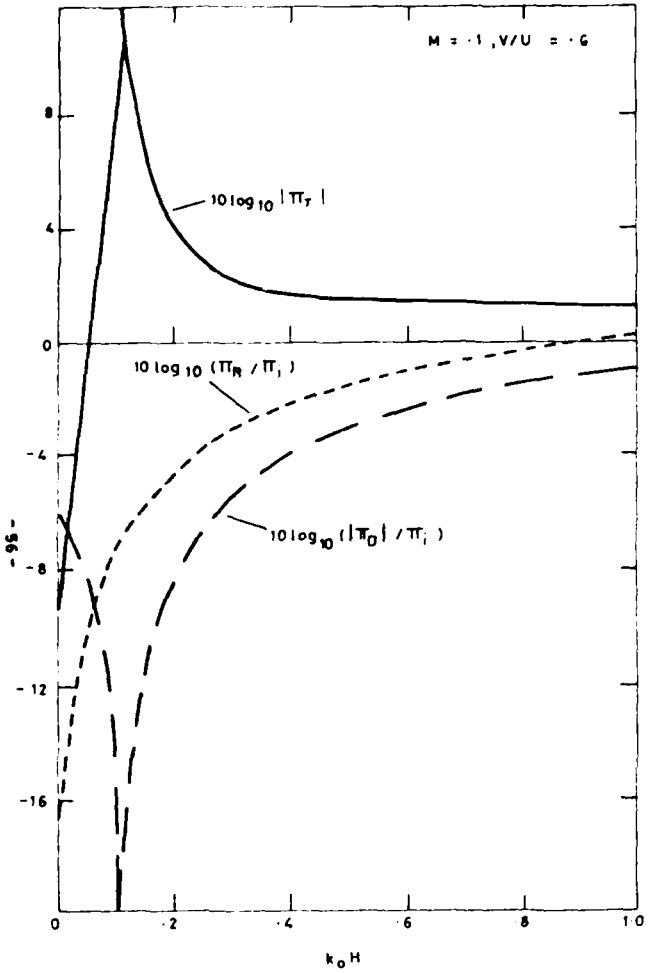

FIG 15 (b)

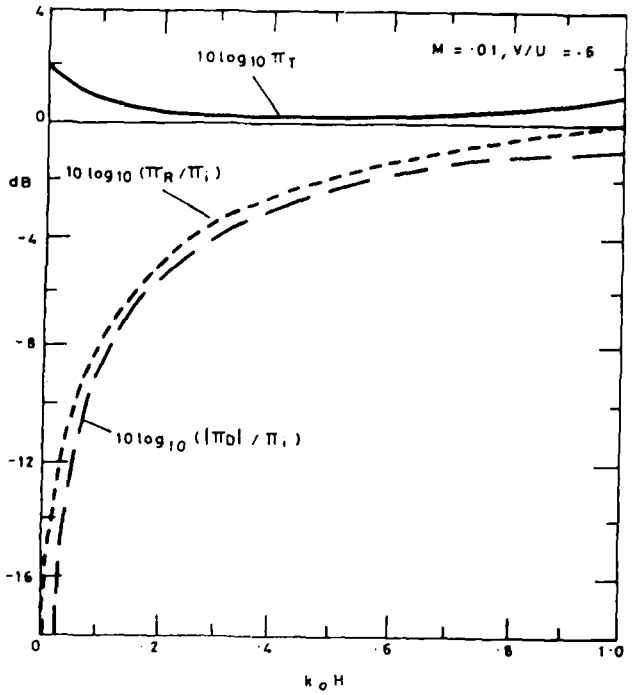

FIG. 15 (c)

direction of the inflow, while for $k_oH > .1$ the net flux is in the incident wave direction. The corresponding results for $M = .01$ are shown in figure 15(c). Figure 16 shows that the net flux of acoustic energy away from the plate edge, $\Pi_R + \Pi_D$, normalized by Π_i is positive as indicated by (3.26).

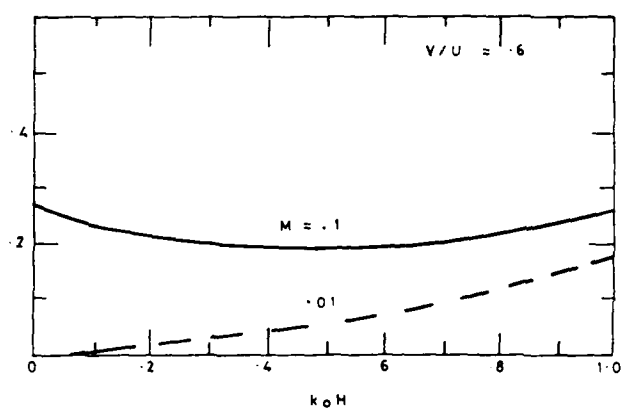

FIG. 16

Figure 16. The net normalized power flux away from the duct mouth $(\Pi_R+\Pi_D)/\Pi_i$, as a function of k_oH with $V/U = .6$ and $M = .1, .01$ as indicated on each curve.

Conlusions

The production of sound when a weak line vortex is convected into a semi-infinite two-dimensional duct by a low Mach number mean flow has been examined by use of a low-frequency Green's function. Howe's theory of displacement thickness fluctuations was applied to model the effect on the radiated sound field of disturbances which are produced by the interaction of the vortex with the leading edge of the duct wall and which propagate in the thin boundary layers emanating from the edge. The strength of the disturbances is fixed by the Kutta condition applied at the leading edge and it is found that the presence of displacement waves reduces the radiated pressure field by a factor of about 4/10 compared to the case in which their presence is ignored.

The duct width, H, is assumed small relative to the characteristic acoustic wavelength d/M, where d is a vorticity length scale and M is the flow Mach number. Analytical expressions are obtained for the far-field, both within and outside the duct. From this solution we find the radiated field produced when a frozen harmonic gust is convected by the duct inflow.

The instantaneous power fluxes of the duct and radiated fields, produced by the interaction of the line vortex with the duct mouth, are compared. We find that the former is of order $\gamma^2 M$ whereas the radiated power flux, an order of magnitude smaller, is proportional to $\gamma^2 M^2$ ($\gamma/2\pi$ is the vortex strength).

The radiation of a plane wave from within the duct has also been examined. The net flux of acoustic energy away from the duct mouth is found to be positive due to a production of acoustic energy by the displacement waves.

ACKNOWLEDGEMENTS

The author is grateful for the comments and advice of Professor P E Doak and Professor M S Howe during the preparation of this report.

M C Quinn, Research Fellow, The Institute of Sound and Vibration Research, Southampton University.

References

Abramowitz, M. & Stegun, I.A. 1964 *Handbook of Mathematical Functions.* Nat. Bur. Stand. appl. Math., Ser. no. 5, Washington D.C..

Blake, W.K. 1970 J. Fluid Mech., 44, 637-660. Turbulent boundary layer wall pressure fluctuations on smooth and rough walls.

Blokhintzev, D.I. 1946. Acoustics of a non-homogeneous moving medium. Leningrad: Gostekizdat (English translation NACA TM 1399).

Bull, M.K. 1967 J. Fluid Mech., 28, 719-754. Wall pressure fluctuations associated with subsonic turbulent boundary layer flow.

Cannel, P. & Ffowcs-Williams, J.E, 1973 J. Fluid Mech., 58, 65-80. Radiation from line vortex filaments exhausting out of a two dimensional semi-infinite duct.

Crighton, D.G., J. Fluid Mech. The operating stages of the jet-edge tone feed-back cycle. (to appear).

Crighton, D.G., 1985 Ann. Rev. Fluid Mech. 17, 411-455. The Kutta condition in unsteady flow.

Davies, P.O.A.L., 1987, J. Sound Vib. 115, 560-564. Plane wave reflection at flow intakes.

Goldstein, M.E., 1981 J. Fluid Mech. 104, 217-246. The coupling between flow instabilities and incident disturbances at a leading edge.

Goldstein, M.E., 1983 J. Fluid Mech. 127, 59-81. The evolution of Tollmein Schlichting waves near a leading edge.

Goldstein, M.E., 1984 J. Fluid Mech. 145, 71-94. Generation of instability waves in flows separating from smooth surfaces.

Gradshteyn, I.S. & Ryzhik, I.M. 1980 *Table of integrals series and products* (corrected edition). New York: Mc Graw Hill.

Howe, M.S. 1975 J. Fluid Mech. 71, 625-673. Contributions to the theory of aerodynamic sound with application to excess jet noise and the theory of the flute.

Howe, M.S. 1981 Proc. R. Soc. Lond., A374, 543-568. The role of displacement thickness fluctuations in hydroacoustics and the jet-drive mechanism of the flue organ pipe.

Lighthill, M.J. 1952 Proc. R. Soc. Lond., A211, 564-587. On sound generated aerodynamically: I General Theory.

Milne-Thompson 1968 *Theoretical Hydrodynamics*. London: Macmillan.

Quinn, M.C & Howe, M.S. 1986 J. Fluid Mech. 168, 1-30. Absorption of sound at a slot in a splitter plate in a mean flow duct.

Figure captions

Figure 1. Schematic illustration of convection of a line vortex by a uniform mean flow into a semi-infinite duct.

Figure 2. Sketch of the idealized boundary layer model with a displacement wave.

Figure 3. Sketch of the control surfaces of equation (2.14) and the vortex wave.

Figure 4. B/A_R of (2.33) as a function of $U_c[t]/H$. h/H is as indicated on each curve and (a) $M_c = .1$; (b) $.001$.

Figure 5. B/A_R of (2.33) plotted against $U_c[t]/H$ for $h/H = .9$ and $M_c = .001, .1, .2$ as indicated on each curve.

Figure 6. B/A_D of (2.35) as a function of $U_c[t]/H$ with $M_c = .1$ and values of h/H as indicated on each curve.

Figure 7. B/A_D of (2.35) plotted against $U_c[t]/H$ for $h/H = .9$ and $M_c = .01, .1, .2$.

Figure 8. Comparison of B/A_R of (2.33) (solid curves) and B/A_D of (2.35) (dashed curves) with $M_c = .1$ and $h/H = .5, .75$ as indicated on each curve.

Figure 9. Illustration of the surfaces in the far-field through which the radiated and duct power fluxes are calculated.

Figure 10. The normalised power fluxes Π_R/W, Π_D/W of (2.50) and (2.52) respectively, plotted in dB against $U_c[t]/H$ with $V/U = .6$ and $M = .1$: (a) $|1-h/H| = .25$; (b) $.1$;

(c) .01.

Figure 11. $10\log_{10}(\Pi_R/I)$ of (2.50) as a function of $U_c[t]/H$ with $V/U = .6$, $M=.1$. h/H is indicated on each curve.

Figure 12. $10\log_{10}(\Pi_R/I)$ (solid curves) and $10\log_{10}(\Pi_D/I)$ (dashed curves) plotted against $U_c[t]/H$ with $V/U = .6$ and $M = .01$, .1, .2, as indicated on each curve.

Figure 13. Radiation of a plane wave from the duct.

Figure 14. The directivity factor of the far-field pressure, D_R of (3.16), as a function of θ, with $V/U = .6$ and (a) $M=.1$; (b) .01. The value of k_oH is indicated on each curve.

Figure 15. The normalized radiated and duct power fluxes, Π_R and Π_D of (3.21), (3.24) respectively, plotted in dB against k_oH with $V/U = .6$ and (a) $M = .1$, $k_oH \leq 4.$; (b) $M = .1$, $k_oH \leq 1.$; (c) $M = .01$, $k_oH \leq 1$.

Figure 16. The net normalized power flux away from the duct mouth $(\Pi_R+\Pi_D)/\Pi_i$, as a function of k_oH with $V/U = .6$ and $M= .1$, .01 as indicated on each curve.

Figure 17. The transformation Z of equation (A1.1).

Figure 18. Sketch of the regions 1-3 around the duct.

Figure 19. Sketch of the flow of equation (A3.4)

Appendix A1 Calculation of a flow transformation and $\bar{\phi}$

The Green's function of (2.11) of the main text, $G(\underline{x};\underline{y})$ is calculated in Appendix A2 for $\underline{x}$ in the far-field. Then when $\underline{y}$ is in the near-field of the duct mouth (BB' of figure 17) $G(\underline{x};\underline{y})$ approximates the potential of an incompressible flow into the duct. Thus the potential $\bar{\phi}$ and stream function $\bar{\psi}$ of the potential flow into the duct which has a uniform velocity of unity in the positive x_1 direction at $x_1 = \infty$, $|x_2| < H$, are required in the calculation of the far-field stagnation enthalpy and are discussed below.

The mapping of the z plane ($z=x_1+jx_2$ and j is the complex imaginary number $(-1)^{\frac{1}{2}}$) consisting of two semi-infinite planes defined by $x_2 = \pm H$, $x_1 > 0$, in the (x_1,x_2) co-ordinate system in figure 17 to the upper half of the Z plane, also sketched in the figure, is found from the Schwarz-Christoffel transformation (Milne-Thompson 1968,§10.2);

$$dz/dZ = K(Z^2-1)/Z \ , \qquad \text{(A1.1)}$$

which gives on integration (with the complex constant K and that of the integration chosen so that the points $(0,\pm H)$ are mapped to $(\pm 1,0)$ in the Z plane)

$$z = (H/\pi)\{ Z^2 -1 -\ln(Z^2) +j\pi \} \ . \qquad \text{(A1.2)}$$

A uniform flow of velocity 1 at $x_1\to\infty$, $|x_2|< H$, is equivalent to a sink at the origin of input 2H taken over an angle π and therefore of strength $2H/\pi$. The complex potential of this flow is w and

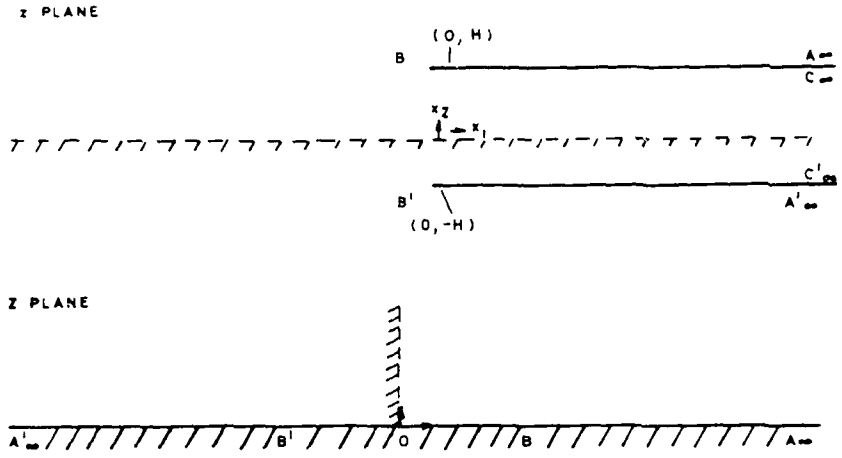

Figure 17. The transformation Z of equation (A1.1).

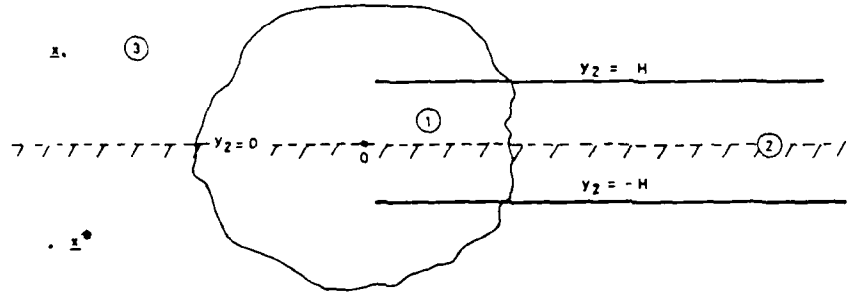

Figure 18. Sketch of the regions 1-3 around the duct.

$$w = -(2H/\pi)\ln(Z) + jH \ , \qquad \text{(A1.3)}$$

and re-arrangement gives

$$Z = +j\exp(-\pi w/2H). \qquad \text{(A1.4)}$$

Substitution for Z in (A1.2) yields

$$z = (H/\pi)(-1 + \exp(-\pi w/H) + w\pi/H) \ . \qquad \text{(A1.5)}$$

The fluid velocity $\underline{u} = (u,v)$ is found from $u - jv = dw/dz$ and

$$dw/dz = 1/(1 + \exp(-\pi w/H)) \ . \qquad \text{(A1.6)}$$

Equating real and imaginary parts in (A1.5) with $w = \phi + j\psi$, we find

$$\begin{aligned} x_1 &= (H/\pi)(-1 + (\phi\pi/H) - \cos(\pi\psi/H)\exp(-\pi\phi/H)) \ , \\ x_2 &= (H/\pi)((\psi\pi/H) + \sin(\pi\psi/H)\exp(-\pi\phi/H)) \ . \end{aligned} \qquad \text{(A1.7)}$$

Approximations for ϕ

On $x_1 > 0$, $x_2 = \pm H$, ψ is constant and $\psi = \pm H$. As $x_1 \to \infty$ with $|x_2| < H$ examination of (A1.7) shows that $\phi \to x_1$. As $|\underline{x}| \to \infty$ outside the duct region of figure A1 we find

$$\phi \to -(H/\pi)\ln(|\underline{x}|\pi/H) \ . \qquad \text{(A1.8)}$$

Expansion of the exponential factors in (A1.7) for $\phi \ll H/\pi$ with $x_2 = H = \psi$ leads to

$$x_1 \simeq (H/2\pi)(\pi\bar{\phi}/H)^2\{\,1+O(\pi\bar{\phi}/H)\}\ ,\ \bar{\phi} \ll H/\pi\ . \qquad \text{(A1.9)}$$

Thus

$$\bar{\phi} \simeq -(\pm(2Hx_1/\pi)^{1/2})\ ,\ x_2 = H\pm 0,\ 0 < x_1 \ll H/\pi\ , \qquad \text{(A1.10)}$$

where the upper/lower signs correspond. The disconinuity in $\bar{\phi}$ across the surface $x_2 = H$, $x_1 > 0$, is approximated by

$$[\bar{\phi}]^{+}_{-} \simeq -2(2Hx_1/\pi)^{1/2}\ ,\ x_1 \ll H/\pi\ . \qquad \text{(A1.11)}$$

Appendix A2. Green's function calculation

Define $G(\underline{x};\underline{y})$ as the solution of

$$\left[\frac{\partial^2}{\partial y_1^2} + \frac{\partial^2}{\partial y_2^2} + \frac{\omega^2}{c^2}\right] G(\underline{x};\underline{y}) = -\delta(\underline{x}-\underline{y})\ , \qquad \text{(A2.1)}$$

which satisfies the boundary conditions

$$\partial G(\underline{x};\underline{y})/\partial y_2 = \begin{cases} 0,\ y_2 = 0,\ |y_1| < \infty, & \text{(A2.2)} \\ 0,\ y_2 = H,\ y_1 > 0\ , & \text{(A2.3)} \end{cases}$$

and the radiation condition that for $|\omega y/c| \gg O(1)$, $G(\underline{x};\underline{y})\exp(-i\omega t)$ should have incoming wave properties with

$$G(\underline{x};\underline{y}) \to A\exp(i\omega y_1/c)\ ,\ y_1 \to \infty,\ |y_2| < H. \qquad \text{(A2.4)}$$

In $\underline{y}$ space $G(\underline{x};\underline{y})$ represents a source with position $\underline{x}$ and will be calculated for $|\underline{x}|$ in the far-field. The boundary condition (A2.2) will be satisfied by placing an image of the semi-infinite plane at $y_2 = -H$, $y_1 > 0$, and an image source at $\underline{x}^* = (x_1, -x_2)$ and requiring instead that $\partial G(\underline{x};\underline{y})/\partial y_2 = 0$ on the image plane. The flow-field around the duct formed by the two planes is divided into three regions (see figure 18). In region 1, $\omega|\underline{y}|/c \ll O(1)$, while $\omega y_1/c > O(1)$, $|y_2| < H$ in region 2 and in region 3 $|\omega\underline{y}/c| > O(1)$. We consider both the case of $\underline{x}$ in the far-field outside the duct and within the duct.

(i) $\underline{x}$ in the far-field outside the duct

Region 3 : The function $G(\underline{x};\underline{y})$ will take the form

$$G(\underline{x};\underline{y}) \rightarrow G_1(\underline{x};\underline{y}) + G_2(\underline{x};\underline{y})$$

where for $|\omega\underline{x}/c| >> 1$

$$G_1(\underline{x};\underline{y}) = (i/4)\{ H_0^{(1)}(\omega|\underline{x}-\underline{y}|/c) + H_0^{(1)}(\omega|\underline{x}^*-\underline{y}|/c) \quad \text{(A2.6)}$$

and

$$G_2(\underline{x};\underline{y}) = \beta H_0^{(1)}(\omega|\underline{y}|/c) \ .$$

$H_0^{(1)}(\underline{x})$ is a Hankel function of the first kind and β is an unknown function of $\underline{x}$. The function $G_1(\underline{x};\underline{y})$ is the solution of (A2.1) when only a plane at $y_2 = 0$ is present while $G_2(\underline{x};\underline{y})$ arises from the presence of the plates and is the far-field produced by the scattering of $G_1(\underline{x};\underline{y})$ by the plate edges. As $|\omega\underline{y}/c| \rightarrow 0$,

$$G_1(\underline{x};\underline{y}) \to a + by_1 ,$$

and (A2.7)

$$G_2(\underline{x};\underline{y}) \to (2\beta/\pi)(i\ln(\omega|\underline{y}|/c) + \pi(.5772-i\ln 2)/2) ,$$

where

$$a = (i/2)H_0(\omega|\underline{x}|/c),\ b = (i\omega x_1/2c|\underline{x}|)H_1(\omega|\underline{x}|/c) , \quad (A2.8a,b)$$

(c.f. Abramowitz and Stegun 1964, p360).

Region 1: Here $|\omega\underline{y}/c|<<1$ and the wave equation (A2.1) is approximated by the Helmholtz equation;

$$\left\{ \frac{\partial^2}{\partial y_1^2} + \frac{\partial^2}{\partial y_2^2} \right\} G(\underline{x};\underline{y}) = 0,\ |\underline{x}| >> |\underline{y}|.$$

$G(\underline{x};\underline{y})$ will be of the form

$$G(\underline{x};\underline{y}) = a + by_1 + \alpha\phi(\underline{y}) + \sigma, \quad (A2.9)$$

where α, σ are as yet undetermined functions of $\underline{x}$ and $\phi(\underline{y})$ is the potential of an incompressible flow which satisfies $\partial\phi/\partial y_2 = 0$ on $y_2=\pm H$, $y_1 >0$ and as $y_1 \to \infty$, $|y_2| < H$, $\phi \to y_1$. ϕ is calcu;ated in Appendix A1 (equation (A1.7). Matchng the far-field form of (A2.9) with the 'outer field' of (A2.6) gives with (A2.7) and result (A1.8) of Appendix A1

$$2\beta(i\ln(\omega|\underline{y}|/c)+\pi/2 +1.5772-i\ln 2) = \alpha(-H\ln(\omega|\underline{y}|/c)+H\ln(\omega H/\pi c))+ \pi\sigma .$$

(A2.10)

Region 2: $G(\underline{x};\underline{y})$ takes the form given in (A2.4) and another equation is obtained by matching the near-field form of that equation to $G(\underline{x};\underline{y})$ of region 1 given by (A2.9) in the limit $\omega y_1/c \to \infty$. In this way we obtain

$$a + by_1 + \alpha y_1 + \sigma = A(1+i\omega y_1/c) \ . \qquad \text{(A2.11)}$$

The equations (A2.10), (A2.11) determine α, β, σ, A in terms of the functions a and b given in (A2.8). We find

$$\alpha = (-b+i\omega a/c)/(1+i(\omega H/\pi c)f(\omega)) \ , \qquad \text{(A2.12)}$$

and

$$\beta = i\alpha H/2 \ , \quad \sigma = -\alpha H f(\omega)/\pi \ , \ A = (\alpha + b)/(i\omega/c). \qquad \text{(A2.13)}$$

where

$$f(\omega) = .5772 + \ln(\omega H/2\pi c) - i\pi/2.$$

(ii) $\underline{x}$ in the far-field within the duct

In a calculation similar to that outlined in (i) above we obtain for A of (A2.4)

$$A = Q + i\exp(-i\omega x_1/c)/(2\omega H/c) \qquad \text{(A2.14)}$$

and

$$Q = \frac{-\hat{R}\exp(i\omega x_1/c)}{2i\omega H/c} \ , \quad R = \frac{-(1-i\omega H f(\omega)/\pi c)}{(1 + i\omega H f(\omega)/\pi c)} \ . \qquad \text{(A2.15a,b)}$$

In region 1 we find that

$$G(\underline{x};\underline{y}) = \alpha\Phi(\underline{y}) + r(\underline{x}), \qquad \text{(A2.16)}$$

where now

$$\alpha = (i\omega B/c) + \exp(i\omega x_1/c)/2H = \frac{1}{H(1+ i\omega Hf(\omega)/\pi c)} \cdot \exp(i\omega x_1/c) \quad , \qquad (A2.17)$$

and $r(\underline{x})$ is a function of $\underline{x}$ which is not needed in the calculation of the main text.

Appendix A3. Complex potential from the boundary layer displacement waves

Define $\bar{G}(\underline{x};y_1)$ as the solution of

$$\left\{ \frac{\partial^2}{\partial x_1^2} + \frac{\partial^2}{\partial x_2^2} - \left[\frac{i\omega}{c} + M\frac{\partial}{\partial x_1} \right]^2 \right\} \bar{G}(\underline{x};y_1) = 0 \ , \qquad (A3.1)$$

which satisfies

$$\partial G/\partial x_2 = \begin{cases} \delta(x_1-y_1), \ x_2 = H\pm 0, \ x_1 > 0, \\ \\ 0, \ x_2 = 0, \ |x_1| < \infty \ . \end{cases} \qquad (A3.2)$$

For $\omega|\underline{x}|/c \ll 1$ and neglecting convection by the mean flow since $M \ll 1$ (A3.1) becomes

$$\left\{ \frac{\partial^2}{\partial x_1^2} + \frac{\partial^2}{\partial x_2^2} \right\} \bar{G}(\underline{x};y_1) = 0 \ , \quad \omega|\underline{x}|/c \ll 1. \qquad (A3.3)$$

If also $\omega|y_1|/c \ll 1$, $\bar{G}(\underline{x};\underline{y})$ represents a line source of strength $\pm 1/\pi$ respectively on the upper/lower side of a rigid plate with a rigid wall a distance H below (see figure 19) in an incompressible fluid. In the Z plane (c.f. Appendix A1, (A1.2)) we find that

$$\bar{G}(\underline{x};\underline{y}) = \mathrm{Re}\{W_a(\underline{x};y_1) + a\} , \quad \omega|x|/c, \ \omega|y_1|/c \ll 1 , \qquad (A3.4)$$

where

$$W_a = \frac{1}{\pi}\ln\left\{\frac{Z^2-Z_+^2}{Z^2-Z_-^2}\right\} + \frac{\lambda}{\pi}\ln(Z^2) . \qquad (A3.5)$$

λ and a are constants. The term in λ accounts for flow at $x_1 = \infty$, $|x_2| < H$ and $Z_\pm$ are the images of the points $y_1+jH\pm 0$ in the Z plane.

At the plate leading edge, $\underline{x} = (0,H)$, $Z = 1$. We find from (A3.5)

$$\left.\frac{dW_a}{dZ}\right|_{Z=1} = \frac{2}{\pi}\left\{\frac{1}{(1-Z_+^2)} - \frac{1}{(1-Z_-^2)}\right\} , \ \omega|y_1|/c \ll 1 . \qquad (A3.6)$$

For y_1 values within a few duct widths of the duct mouth λ is small and has been neglected in (A3.6) where the remaining terms are (c.f Appendix A1) of order $(\pi y_1/H)^{-m}$ for $y_1 \ll H$. The component of the perturbation potential due to the presence of displacement waves on the boundary layers of the plate at $x_2 = H\pm 0$, $x_1 > 0$ can, in view of (A3.1), (A3.2) and equation (2.8) of the main text be expressed as a complex potential, W_b say, in the near-field of the plate leading edge with

$$W_b = \Psi(\omega)\int_0^\infty W_a(\underline{x};y_1)\exp(i\chi y_1 - i\omega t)\, dy_1 , \quad \omega|x|/c \ll 1. \qquad (A3.7)$$

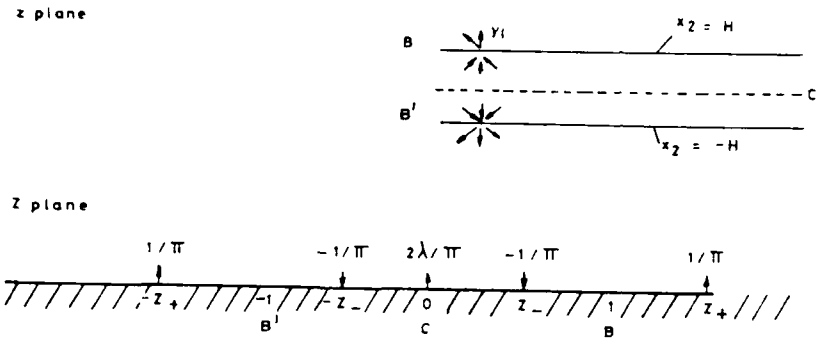

Figure 19. Sketch of the flow of equation (A3.4)

Appendix A4. To determine $\psi(\omega)$ by application of the Kutta condition.

The perturbation potential due to the vorticity wave ω_1 ((2.4b) of the main text) will, in the vicinity of the plate edge (0,H), approximate that of an incompressible flow which has a complex potential W_a where

$$W_a = \frac{-j\,\gamma\,\exp(i\omega(t_o-t))}{2\pi(2\pi U_c)}\int_{-\infty}^{\infty}\ln\left\{\frac{Z-Z_o}{Z-Z_o^*}\right\}\exp(i\omega y_1/U_c)dy_1$$

$$\frac{-j\,\gamma\,\exp(i\omega(t_o-t))}{2\pi(2\pi U_c)}\int_{-\infty}^{\infty}\ln\left\{\frac{Z+Z_o}{Z+Z_o^*}\right\}\exp(i\omega y_1/U_c)dy_1\ . \qquad (A4.1)$$

Z_o is the image of the point y_1+jh under the mapping (A1.2) of Appendix A1. The second integral on the right hand side of (A4.1) accounts for the image of the vortex wave in the wall at $x_2 = 0$. The total potential in the vicinity of the edge (0,H) has complex potential W say, where from Appendix A3, (A3.9) and (A3.4)

$$W = W_a + W_b. \qquad (A4.2)$$

W_b arises from the boundary layer displacement waves while W_a is due directly to the vorticity wave. The fluid velocity at the leading edge of the plate is

$$\left.\frac{dW}{dz}\right|_{y,H} = \left\{\frac{d\,(W_a + W_b)}{dZ}\,\frac{dZ}{dz}\right\}\Bigg|_{Z=1},$$

$$= [(\pi/2H)(d(W_a + W_b)/dZ)/(Z^2-1)]|_{Z=1}\ , \qquad (A4.3)$$

(c.f. (A1.2) of Appendix A1). For the fluid velocity to remain finite at the edge we require that

$$d(W_a + W_b)/dZ = 0 , \quad Z = 1. \tag{A4.4}$$

From equations (A3.6), (A3.9) of Appendix A3 we obtain for $Im(\chi) > 0$

$$(dW_b/dZ)|Z=1 = -2(\Psi(\omega)/\pi)\exp(-i\omega t)\int_{-\infty}^{\infty}\exp(i\chi y_1)d\phi\Big|_{\Psi=H} , \tag{A4.5}$$

where the integration variable is the potential ø and (A1.4), (A1.6) of Appendix A1 have been used. With (A1.7) of Appendix A1 and Gradshteyn and Ryzhik (1980, p308) we find

$$(dW_b/dZ)|Z=1 = -2(\Psi(\omega)H/\pi^2)\exp[L(-i\chi H/\pi)] , \tag{A4.6}$$

where

$$L(x) = \ln\Gamma(x) - x\ln x + x . \tag{A4.7}$$

$\Gamma(x)$ is the gamma function (Gradshteyn and Ryzhik 1980, p933).

Differentiation of (A4.1) gives

$$\left.\frac{dW_a}{dZ}\right|_{Z=1} = (2/\pi U_c)(\gamma/2\pi)\exp(i\omega(t_o-t))K , \tag{A4.8}$$

where

$$K = \int_{-\infty}^{\infty}\exp(i\omega y_1/U_c)\,Im[\,1/(1-Z_o^2)]\,dy_1 . \tag{A4.9}$$

Im(f) denotes the imaginary part of f and Z_o is the image of y_1+jh in the Z plane. Condition (A4.4) becomes with (A4.7), (A4.8)

$$\nu(\omega) = (\gamma/2HU_c)\exp[i\omega t_o - L(-i\chi H/\pi)]\mathcal{K} . \qquad (A4.10)$$

To evaluate $\mathcal{K}$

Note that (c.f. Appendix A1, (A1.4), (A1.6))

$$\mathcal{K} = T(\omega) + T^*(-\omega) , \qquad (A4.11)$$

where

$$T(\omega) = \frac{-i}{2}\exp(\omega h/U_c)\int_{-\infty}^{\infty}\frac{dw}{dz}\exp(i\omega z/U_c)dz\Big|_{z=y_1+jH} . \qquad (A4.12)$$

w is the complex potential of Appendix A1. T is evaluated as an integral in the complex z plane of figure 17 and with (A1.7) of Appendix A1 and Gradshteyn and Ryzhik 1980 (p307, p942) we obtain

$$\mathcal{K} = \begin{cases} -i(H/\pi)\exp[L(i\omega H/\pi U_c)]\sinh(\omega h/U_c)\exp(-\omega H/U_c) , & h < H, \\ -i(H/\pi)\exp[L(-i\omega H/\pi U_c)]\sinh(\omega H/U_c)\exp(-\omega h/U_c) , & h > H , \end{cases} \qquad (A4.13)$$

In the limit $\omega H/U_c >> 1$, when the duct height is extremely large relative to the hydrodynamic length scale U_c/ω, use of the asymptotic form of L (c.f Gradshteyn and Ryzhik 1980, p940) gives for $\omega > 0$

$$K(\omega) = \begin{cases} (1-i)(U_c H/\omega)^{1/2}\sinh(\omega h/U_c)\exp(-\omega H/U_c) \ , & h < H, \\ (1-i)(U_c H/\omega)^{1/2}\sinh(\omega H/U_c)\exp(-\omega h/U_c) \ , & h > H, \end{cases} \tag{A4.14}$$

correct to neglect of terms of order $(U/\omega H)$ relative to unity.

Calculation of $\nu(\omega)$ in the case of plane wave radiation from the duct.

In the case of a long wavelength sound wave radiating from the duct the perturbation potential in the absence of displacement waves is ϕ_d and in the vicinity of the leading edge of the plate it can be treated as the potential of an incompressible flow. The complex potential of this flow will be of the form $\mu w(z)$, where $w(z)$ is given by (A1.3) of Appendix A1 and represents flow into the duct which becomes uniform with speed unity well within the duct. μ is chosen to match the near field of the x_1 velocity of the incident and reflected waves, $\phi_i+\phi_r$ of (3.9), i.e. $\mu = \partial(\phi_i+\phi_r)/\partial x_1$ in the limit $k_0 x_1 \to 0$. Neglecting order M^2 relative to unity we find from (3.9), (3.1) of the main text

$$\mu = -ik_0\phi_0(1-R+M(R+1)). \tag{A4.15}$$

$\nu(\omega)$ is found from condition (A4.4) and (A4.7) with W_d now equal to $\mu w(z)$ and (c.f(A1.3) of Appendix A1)

$$\left.\frac{dW_d}{dZ}\right|_{Z=1} = -2\mu H/\pi \ .$$

We find for $\nu(\omega)$

$$\nu(\omega) = -(1-i)\mu(|\chi|H)^{1/2}/2 \ ,$$

$$= i(1-i)k_0\phi_0(|\chi|H)^{1/2}(1-R+M(1+R))/2 \ . \tag{A4.16}$$

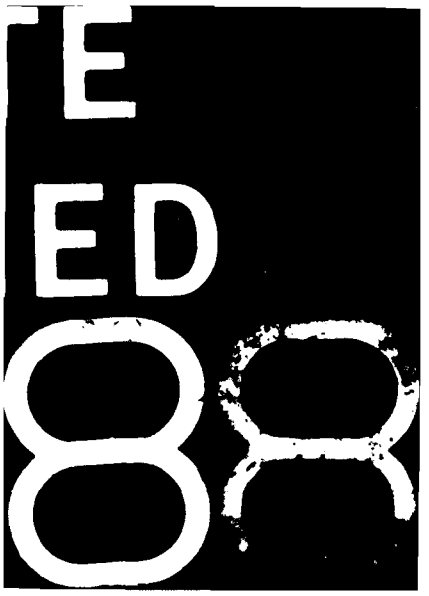
E
ED
80